J Physiol 593.19 (2015) pp 4341–4360

JPn Neuroscience

The Journal of Physiology

The extracellular matrix molecule brevican is an integral component of the machinery mediating fast synaptic transmission at the calyx of Held

Maren Blosa[1], Mandy Sonntag[1,2], Carsten Jäger[1], Solveig Weigel[1], Johannes Seeger[3], Renato Frischknecht[4], Constanze I. Seidenbecher[4], Russell T. Matthews[5], Thomas Arendt[1], Rudolf Rübsamen[2] and Markus Morawski[1]

[1] *Paul Flechsig Institute for Brain Research, Faculty of Medicine, University of Leipzig, 04103 Leipzig, Germany*
[2] *Institute of Biology, Faculty of Biology, Pharmacy and Psychology, University of Leipzig, 04103 Leipzig, Germany*
[3] *Institute of Anatomy, Histology and Embryology, Faculty of Veterinary Medicine, University of Leipzig, 04103 Leipzig, Germany*
[4] *Leibniz Institute for Neurobiology, 39118 Magdeburg, Germany*
[5] *Department of Neuroscience and Physiology, State University of New York Upstate Medical University, Syracuse, NY 13210, USA*

Key points

- The proteoglycan brevican is a major component of the extracellular matrix of perineuronal nets and is highly enriched in the perisynaptic space suggesting a role for synaptic transmission.
- We have introduced the calyx of Held in the auditory brainstem as a model system to study the impact of brevican on dynamics and reliability of synaptic transmission.
- *In vivo* extracellular single-unit recordings at the calyx of Held in brevican-deficient mice yielded a significant increase in the action potential (AP) transmission delay and a prolongation of pre- and postsynaptic APs.
- The changes in dynamics of signal transmission were accompanied by the reduction of presynaptic vGlut1 and ultrastructural changes in the perisynaptic space.
- These data show that brevican is an important mediator of fast synaptic transmission at the calyx of Held.

Abstract The extracellular matrix is an integral part of the neural tissue. Its most conspicuous manifestation in the brain are the perineuronal nets (PNs) which surround somata and proximal dendrites of distinct neuron types. The chondroitin sulfate proteoglycan brevican is a major component of PNs. In contrast to other PN-comprising proteoglycans (e.g. aggrecan and neurocan), brevican is mainly expressed in the perisynaptic space closely associated with both the pre- and postsynaptic membrane. This specific localization prompted the hypothesis that brevican might play a role in synaptic transmission. In the present study we specifically investigated the role of brevican in synaptic transmission at a central synapse, the calyx of Held in the medial nucleus of the trapezoid body, by the use of *in vivo* electrophysiology, immunohistochemistry, biochemistry and electron microscopy. *In vivo* extracellular single-unit recordings were acquired in brevican-deficient mice and the dynamics and reliability of synaptic transmission were compared to wild-type littermates. In knockout mice, the speed of pre-to-postsynaptic action potential (AP) transmission was reduced and the duration of the respective pre- and postsynaptic APs increased. The reliability of signal transmission, however, was not affected by the lack of brevican. The changes in dynamics of signal transmission were accompanied by the reduction of (i) presynaptic vGlut1 and (ii) the size of subsynaptic cavities. The present results suggest an essential role of brevican for the functionality of high-speed synaptic transmission at the calyx of Held.

M. Blosa and M. Sonntag contributed equally to this work.

DOI: 10.1113/JP270849

(Resubmitted 30 April 2015; accepted after revision 20 July 2015; first published online 30 July 2015)
Corresponding author M. Morawski: Paul Flechsig Institute for Brain Research, Faculty of Medicine, University of Leipzig, Liebigstrasse 19, 04103 Leipzig, Germany. Email: morm@medizin.uni-leipzig.de

Abbreviations ANF, auditory nerve fibre; AP, action potential; AVCN, anterior ventral cochlear nucleus; CF, characteristic frequency; CNS, central nervous system; ECM, extracellular matrix; EPSP, excitatory postsynaptic potential; LSO, lateral superior olive; MNTB, medial nucleus of the trapezoid body; PN, perineuronal net; SNR, signal-to-noise ratio; VCN, ventral cochlear nucleus; vGlut, vesicular glutamate transporter.

Introduction

In the central nervous system (CNS), specific neurons are surrounded by distinct extracellular matrix (ECM) components collectively termed the 'perineuronal net' (PN). Over the years, a wide range of functions have been assigned to PNs. These include (i) stabilization of synaptic contacts and (ii) control of synaptic activity and CNS plasticity (Kantor *et al.* 2004; McRae *et al.* 2007; Vigetti *et al.* 2008; Hrabetová *et al.* 2009). The structure of PNs is based on the interplay of different molecules. The main components are chondroitin sulfated proteoglycans complexed with hyaluronan, tenascin-R and link protein forming a quaternary complex organized in region- and cell type-dependent patterns (Yamaguchi, 2000; Morawski *et al.* 2014). The PN components typically surround the entire somata of the neurons and the contacting synaptic terminals. However, one exception is the proteoglycan brevican, which is expressed mainly in the perisynaptic space tightly associated with both, the pre- and postsynaptic membranes (Frischknecht & Seidenbecher, 2012; Blosa *et al.* 2013). This specific spatial arrangement suggests that brevican might influence synaptic transmission (Brakebusch *et al.* 2002; Blosa *et al.* 2013). The present study aims at testing this hypothesis by investigating the properties of synaptic transmission at the calyx of Held synapse in the medial nucleus of the trapezoid body (MNTB) in mice that are deficient in brevican (Brakebusch *et al.* 2002). The calyx of Held is formed on the somata of MNTB principal neurons, virtually all of which are surrounded by PNs (Blosa *et al.* 2013; Sonntag *et al.* 2015). The calyces of Held constitute exceptionally large, glutamatergic terminals which cover ∼50% of postsynaptic neurons. Due to their huge size, they have become a favourite model system for studying synaptic transmission in the central nervous system (Gersdorff & Borst 2002; Schneggenburger & Forsythe 2006) and they are also particularly suited for a detailed investigation of any physiological function of PNs (Blosa *et al.* 2013).

Young adult animals (P23–P31) were used in the present study to assure mature configuration of PNs, which is not reached before the end of the third postnatal week. The mature calyx of Held is characterized by extremely fast and highly reliable synaptic transmission, which is connected with its specific function within the auditory circuitry. This is why the study focused on the contribution of brevican to the dynamics and reliability of synaptic transmission at the calyx of Held. Extracellular single-unit recordings were acquired *in vivo,* which enables the simultaneous acquisition of both, the pre- and postsynaptic activity of MNTB principal cells. This way, the temporal relation between the input and output is preserved, which allows for direct quantification of transmission reliability and for real-time analysis of the dynamics of pre-to-postsynaptic signal transmission. At the current state of our knowledge about the contribution of PNs to synaptic transmission, we refrained from using apparently obvious brainstem slice recordings for a number of technical constraints in adult animals: after the third postnatal week, brainstem nuclei (i) are strongly myelinated and (ii) show a dense accumulation of extracellular matrix around the neurons, which provide extremely difficult conditions for high-quality whole-cell patch-clamp recordings in brainstem slices (Morales *et al.* 2004; Borst 2010). Also, the loss of spontaneous activity in brainstem slices has a long lasting influence on synaptic physiology (Hermann *et al.* 2007; Lorteije *et al.* 2009; Borst 2010; Klug 2011). *In vivo* recordings on the other hand establish a lower level of reduction and – at the same time – enable the acquisition of elaborate data on distinct properties of synaptic transmission including dynamics, reliability and activity-dependent modulation (Englitz *et al.* 2009; Lorteije *et al.* 2009; Tolnai *et al.* 2009; Sonntag *et al.* 2011). Also, simultaneous intra- and extracellular recordings of MNTB principal neurons and bushy cells in the anterior ventral cochlear nucleus (AVCN) have shown that activity acquired extracellularly reliably indicates intracellular voltage changes (Lorteije *et al.* 2009; Typlt *et al.* 2010).

The present results show that in brevican knockout mice both the pre- and the postsynaptic action potentials (AP) are broadened and the speed of synaptic transmission is significantly reduced. The reliability of synaptic transmission, however, is not altered. Characterization of calyx synapses and MNTB principal cells by means of immunohistochemistry yielded no differences in the expression of potassium channels, calcium channels and AMPA receptors, all of which promote fast signal transmission at the calyx of Held. Also, the typical highly fenestrated morphology of the calyx of Held is

not affected in knockout mice. On the ultrastructural level, however, significantly reduced sizes of subsynaptic cavities were observed between the pre- and postsynaptic membranes. Additionally, a reduced amount of vGlut1 was found, pointing towards an involvement of brevican in glutamatergic signalling. These results provide strong evidence that brevican is an integral component of the machinery mediating fast synaptic transmission at the calyx of Held.

Methods

Ethical approval

All experiments were performed in agreement with the German law on the use of laboratory animals, followed the ethical guidelines of the laboratory animal care and use committee at the University of Leipzig, and were approved by the Saxonian District Government, Leipzig (TVV 66/13).

Animals

Homozygous brevican-deficient mice ($bcan^{-/-}$) and wild-type littermates ($bcan^{+/+}$) on the C57BL/6 background (Rauch *et al.* 1997; Brakebusch *et al.* 2002) were used in the experiments. The genotype of each experimental animal was determined by PCR genotyping and confirmed by brevican immunohistochemistry. The animals were bred in the animal care facility of the Paul-Flechsig-Institute for Brain Research of the University of Leipzig and kept on a 12 h–12 h dark–light cycle with free access to food and water. Experiments were performed on young adult mice of both sexes between postnatal days 23 and 31 (P23–P31), an age range at which PNs in the MNTB are fully developed (Blosa *et al.* 2013).

Immunohistochemistry

Immunohistochemistry was used to (i) characterize the composition of perineuronal nets, (ii) characterize the expression of ion channels and receptors, and (iii) quantify the expression of the vesicular glutamate transporter 1 and 2 (vGlut1 and vGlut2) and the glutamate uptake transporter GLT1. For each of these approaches we used three $bcan^{+/+}$ and three $bcan^{-/-}$ mice (P24–30). The animals were anaesthetized with CO_2 and perfused transcardially with 0.9% NaCl followed by fixative (4% paraformaldehyde and 0.1% glutaraldehyde). Brains were removed, postfixed overnight, and cryoprotected in 30% sucrose with 0.1% sodium azide before cutting 30 μm thick slices in the frontal plane with a cryomicrotome (Zeiss Hyrax S30 with freezing unit Zeiss Hyrax KS34). Before staining, the slices were treated with 60% methanol and 2% H_2O_2 for 1 h, followed by blocking solution (2% bovine serum albumin (BSA), 0.3% milk powder and 0.5% donkey serum) for 30 min. The antibodies are summarized in Table 1. All antibodies were incubated in blocking solution for 2 days at 4°C and visualized by fluorescent secondary antibodies (Table 2).

Tissue sections were imaged using a Zeiss confocal laser-scanning microscope (LSM 510, Zeiss, Jena, Germany) and a Keyence fluorescence microscope (BZ-9000, Keyence, Neu-Isenburg, Germany). Photoshop CS2 (Adobe Systems, San Jose, CA, USA) was used to adjust contrast and background.

Quantification of vGlut1, vGlut2 and GLT1

From the region of the MNTB, every second slice was double-stained with neurocan and either vGlut1, vGlut2 or GLT1. All slices from all animals used for quantification were processed in a single experimental approach to achieve a high degree of comparability between staining of different animals. The respective MNTB of each side was analysed separately and the entire rostrocaudal dimension of the nuclei was included.

A Keyence BZ-9000 microscope was used for microscopic analyses and acquisition of digital images. Images were acquired using equal exposure values for each fluorescence channel. From different MNTB areas, stacks of images comprising seven planes at distances of 3 μm were gathered and collapsed into single full focus images. Quantification was performed with the Keyence BZ II Analyser software using the Hybrid Cell Count tool (Keyence, Biorevo, Neu-Isenburg, Germany). Firstly, the neurocan image was visualized and the PN-rich area, indicating the location and the dimensions of the MNTB, was marked with a drawing tool. Secondly, the corresponding vGlut1, vGlut2 or GLT1 images were visualized and the neurocan stained cellular components within the nuclear area were quantified. Settings of brightness were adapted within a fixed range of values (defined in a test series) so that the whole of the neurocan-labelled MNTB area stood out visually. The analysis provided numeric values of the neurocan-stained fraction within the area of the MNTB, indicating the respective density of vGlut1, vGlut2 and GLT1 immunoreactivity.

Anterograde labelling of the calyx of Held

Four young adult mice (2 $bcan^{+/+}$, 2 $bcan^{-/-}$, P24–P27) were anaesthetized with CO_2 and perfused transcardially as described above. Brains were removed and postfixed overnight. Projections from the ventral cochlear nucleus

Table 1. Histochemical markers used for detection of extracellular matrix components, channel proteins, receptor proteins and transmitters

Detected components	Antibodies/binding proteins	Dilution		Source	References
Matrix constituents		IHC	WB		
Aggrecan, core protein (aa 1177–1326; AB1031)	Rabbit anti-aggrecan		1:1000	Millipore	Brückner *et al.* 2006
Aggrecan, core protein (HAG7D4)	Mouse anti-human aggrecan	1:10		Serotec	(Brückner *et al.* 2008)
Brevican (50 kDa cleavage fragment)	Rabbit anti-human brevican	1:2000		R.T. Matthews	(Matthews *et al.* 2000)
Neurocan, N-terminal part (MAB 5212)	Sheep anti-neurocan	1:500	1:2500	R&D Systems	(Milev *et al.* 1998)
Brevican (aa 232–394)	Mouse anti-brevican	1:1000		BD Bioscience	(Vitellaro-Zuccarello *et al.* 2007)
Channel proteins					
Voltage-gated calcium channel $Ca_v1.2$	Rabbit anti-$Ca_v1.2$	1:200		Alomone Labs	(Lv *et al.* 2014)
Voltage-gated calcium channel $Ca_v1.3$	Rabbit anti-$Ca_v1.3$	1:200		Alomone Labs	(Pirone *et al.* 2014)
Voltage-gated calcium channel $Ca_v2.1$	Rabbit anti-$Ca_v2.1$	1:200		Millipore	(Mallmann *et al.* 2013)
Voltage-gated potassium channel $K_v1.3$	Rabbit anti-$K_v1.3$	1:300		Alomone Labs	(Gazula *et al.* 2010)
Voltage-gated potassium channel $K_v1.6$	Rabbit anti-$K_v1.6$	1:400		Alomone Labs	(Gazula *et al.* 2010)
Voltage-gated potassium channel $K_v2.2$	Rabbit anti-$K_v2.2$	1:500		Alomone Labs	(Tong *et al.* 2013)
Voltage-gated potassium channel $K_v3.1\beta$	Rabbit anti-$K_v3.1$ß	1:800		Alomone Labs	(Härtig *et al.* 1999)
Voltage-gated potassium channel $K_v3.1\beta$	Mouse anti-$K_v3.1$ß	1:300		NeuroMab	(Tong *et al.* 2013)
Receptor proteins					
C-terminal part of GluR2 and GluR3	Rabbit anti-GluR 2/3	1:100		Chemicon	(Thiers *et al.* 2008)
AMPA receptor (GluR4) protein	Rabbit anti-GluR4	1:500		Cell Signaling	(Caicedo and Eybalin, 1999)
NMDA receptor subunit NMDAR2A	Rabbit anti-NMDAR2A	1:1000		Millipore	(Kim *et al.* 2008)
Transmitters					
Glutamate transporter 1	Guinea pig anti-vGlut1	1:500		Synaptic Systems	(Takamori *et al.* 2000)
Glutamate transporter 2	Guinea pig anti-vGlut2	1:250		Synaptic Systems	(Takamori *et al.* 2000)
Glial Glutamate transporter 1, C-terminal part (AB1783)	Guinea pig anti-Glt-1	1:1000		Millipore	(Pines *et al.* 1992)
Reference protein					
Heat shock protein 90 kDa	Rabbit anti-HSP90	1:1000	1:1000	Cell Signaling	(Suttkus *et al.* 2014)

(VCN) to MNTB were labelled with the lipophilic dye NeuroVue Red (PTI Research, Warrington, PA, USA) (Hsieh & Cramer 2006; Nakamura & Cramer 2013). Briefly, a small piece of dye-filter-tip was inserted into the brain at the location of the VCN, which stands out at the lateral surface of the brainstem. The preparation was kept for 5 weeks in 4% paraformaldehyde at 37°C to allow the dye to diffuse along the axons to the synaptic terminals in the MNTB. Seventy-five micrometre thick brain slices were cut as described above. Labelled calyces of Held were imaged by a Zeiss confocal laser scanning microscope (LSM 510, Zeiss, Jena, Germany).

To evaluate the degree of fenestration of the calyx of Held synapses, we classified the terminals according to the five categories introduced by Ford *et al.* (2009): cup-like shaped (category 1), early fenestrated (category 2, closed area covering about 60–80% of calyx surface), intermediate fenestrated (category 3, closed area covering

Table 2. Secondary antibodies

Antibody	Labelling	Dilution	Source
Donkey anti-guinea pig	Cy5	1:200	Dianova
Donkey anti-goat	Cy2	1:200	Dianova
Donkey anti-goat	Cy5	1:200	Dianova
Donkey anti-mouse	Cy2	1:200	Dianova
Donkey anti-mouse	Cy3	1:250	Dianova
Donkey anti-rabbit	Cy3	1:250	Dianova
Donkey anti-rabbit	IgG	1:10000	GE Healthcare
Rabbit anti-goat	IgG	1:10000	Dako

about 50% of calyx surface), late fenestrated (category 4, closed area reduced to 10–25% of calyx surface), and completely fenestrated (category 5).

Electron microscopy

Four young adult mice (2 *bcan*$^{+/+}$, 2 *bcan*$^{-/-}$, P30) were perfused as indicated above but using a modified fixative containing 2% formaldehyde and 2% glutaraldehyde. Brains were removed and post-fixed overnight at 4°C in the same solution. Vibrating-blade microtome sections (50 μm) were taken at the level of the MNTB according to the stereotaxic atlas of Franklin & Paxinos (1997).

Brain tissue blocks which included the MNTB were dissected from the vibrating-blade microtome sections, post-fixed in buffered 1% osmium tetroxide at room temperature for 1 h, rinsed in phosphate-buffered saline (PBS), dehydrated in a graded series of acetone and embedded in Glycidether100 resin (formerly Epon 812; Carl Roth, Karlsruhe, Germany). For structural orientation, semi-thin sections were cut at 1 μm thickness and stained with toluidine blue. Ultrathin sections were cut on an Ultracut UCT (Leica Microsystems, Wetzlar, Germany). Sections were examined with a Zeiss 912 Omega and EFTEM Libra 120 transmission electron microscope (Zeiss, Oberkochen, Germany). Digital images were captured with a Sharpeye 1k CCD camera (TRS; Troendle, Munich, Germany). Data were obtained from 18 MNTB sections taken from different neurons in two *bcan*$^{+/+}$ mice and from 28 MNTB sections taken from different neurons in two *bcan*$^{-/-}$ mice. Due to the huge size of the calyx of Held, only small fractions of the synaptic terminals (defined as 'profiles' according to Ryugo *et al.* 2006) are visible in the ultrathin sections. In both genotypes, the synaptic profiles were examined with respect to the numbers and sizes of subsynaptic cavities, a morphological entity defined as extracellular spaces occurring between the opposing pre- and post-synaptic membranes underneath the calyx of Held. The sizes of the cavities were measured by outlining the edges of the respective structures with a drawing tool and calculating the area within the perimeter. Only cavities with a minimum lateral extension of 100 nm were included in the analysis (Ryugo *et al.* 2006). In total, 18 calyx of Held profiles and 88 cavities were analysed in *bcan*$^{+/+}$ mice and 30 calyx of Held profiles and 152 cavities in *bcan*$^{-/-}$ mice. To compare between the genotypes and to compensate for different extensions of calyx of Held profiles in the different ultrathin sections, the number of cavities was normalized to the length of the respective calyx of Held profile. Quantification of subsynaptic cavities was performed using ITEM analysis Software (Olympus, Münster, Germany).

Western blot

Western blotting was used to additionally investigate potential quantitative differences in protein expression levels of aggrecan and neurocan. Untreated brains of five *bcan*$^{+/+}$ and five *bcan*$^{-/-}$ mice (P28) were removed from the skull and immediately shock frozen in liquid nitrogen. Deep-frozen brains were cut into 2 mm thick frontal sections. The part of the brainstem tissue including the auditory brainstem nuclei was isolated from the section and homogenized with 5× volume of homogenizing buffer and complete protease inhibitor (Roche) using the Ultra Turaxx mixer unit. After centrifugation of the homogenate at 10,000 *g* for 15 min at 4°C, the supernatant was decanted. For analysis of the core proteins of neurocan and aggrecan, 100 μl of the supernatant (~700 μg total protein) was digested with 0.05 units chondroitinase (Sigma-Aldrich, according to Matthews *et al.* 2002) in Tris-HCl (pH 8.0) containing complete protease inhibitor for 3.5 h at 37°C and denatured with the same volume of Laemmli sample buffer at 70°C for 15 min. Proteins (35 μg per lane) were electrophoretically separated in a 6% SDS-PA gel and electrotransferred onto a polyvinylidene difluoride membrane (Roche) overnight at constant 30 V. After blocking with 1% BSA in TBS-T (0.05% Tween-20), the PVDF membrane was incubated with the primary antibodies overnight at 4°C (see Table 1) and subsequently washed three times for 10 min with TBS-T. The blot was treated with a 1:10,000 diluted peroxidase conjugated antibody for 1 h (see Table 2). Heat shock protein (HSP90) was used as a reference protein for quantification. The optical density of protein bands was finally detected with an enhanced chemoluminescence detection system (DNR Bio-Imaging system, Biostep, Germany) and evaluated using TINA software (Raytest, Germany).

In vivo single-unit recordings

In vivo single-unit recordings were performed in five *bcan*$^{+/+}$ and five *bcan*$^{-/-}$ mice (P23–P31).

Surgical preparation. The mice were deeply anaesthetized by an initial injection of a mixture of ketamine hydrochloride (0.1 mg per g body weight, Ratiopharm) and xylazine hydrochloride (0.005 mg per g body weight, Bayer). A constant level of anaesthesia was maintained during the experiments by giving supplementary injections of one-third of the initial dose. Animals were fixed in a stereotaxic recording device through a small metal bolt which was glued onto the prefrontal skull. Two holes with a diameter of 500 μm were drilled in the skull to insert the recording and the reference electrodes. The two holes were located 2000 μm caudal to the lambda suture with the one for the recording electrode directly at the midline and the one for the reference electrode about 1500 μm lateral to the midline. The MNTB was reached at a depth of $\sim$5500 μm (for details of the surgical procedure see Sonntag *et al.* 2009).

Data collection. During the electrophysiological measurements the animals were positioned in a sound attenuated chamber (type 400; Industrial Acoustics, Niederkrüchten, Germany) on a vibration-isolated table. The body temperature was kept at $\sim$37°C by a temperature-controlled heating pad. Single-unit activity was acquired by using glass electrodes filled with 3 M KCl (5–10 MΩ). MNTB principal neurons were identified by their characteristic complex voltage signals which comprise the activity of the calyx of Held and its corresponding MNTB principal neuron (Guinan & Li, 1990; Kopp-Scheinpflug *et al.* 2003; Lorteije *et al.* 2009; Sonntag *et al.* 2009). The recorded voltage signals were amplified (Neuroprobe 1600, A-M Systems, Sequim, WA, USA and PC1, Tucker-Davis Technologies, Alachua, FL, USA) and digitized by an A/D converter (RP2.1, Tucker-Davis Technologies) at a sampling rate of 97.7 kHz. The voltage traces were bandpass filtered (50–7000 Hz) using a custom-written MATLAB software (The MathWorks, Ismaning, Germany).

For each MNTB unit, spontaneous activity was recorded for 150–300 s. For estimation of the units' characteristic frequencies (CF), thresholds and maximum sound-evoked discharge rates, the following stimulation protocol was used: The frequency response area was measured based on randomized presentation of 100 ms pure tones within a predefined range of 20 $\times$ 10 frequency/intensity combinations (rise–fall time 5 ms, interstimulus interval 100 ms). Each frequency–intensity pair was presented five times. The CF was defined as the stimulus frequency associated with the lowest response threshold, and the maximum firing rate was defined as the highest discharge rate elicited by one of the 200 presented frequency–intensity combinations.

Acoustic stimulation. Custom-written MATLAB software was used for generation of acoustic stimuli. The signals were transferred to a D/A converter (RP2.1, Tucker-Davis Technologies; sampling rate: 97.7 kHz) and presented via custom-made earphones (DT 770 pro, Beyerdynamic) equipped with plastic tubes (diameter: 5 mm; length: 70 mm) that were placed just in front of the eardrum.

Data analysis. Extracellular single-unit recordings in the MNTB yielded complex voltage signals which were used to quantify the dynamics and reliability of synaptic transmission. Signal complexes were characterized by an initial positive deflection, indicating the action potential of the calyx of Held (preAP), followed by the EPSP of the MNTB principal neuron, which can – to different degrees – segue into the subsequent postsynaptic action potential (postAP) (Lorteije *et al.* 2009; Sonntag *et al.* 2011). Signal complexes were extracted from a given recording by using custom-written MATLAB software (Sonntag *et al.* 2009). The signals were spike-sorted based on principal component analysis followed by hierarchical cluster analysis. Only recordings with constant shapes and amplitudes of the complex waveforms (<20% variation) and a signal-to-noise ratio (SNR, defined as the maximum positive peak divided by the standard deviation of the noise) of the preAP exceeding 2.5 were included in the analysis. The average SNR of the preAP was 5.1 $\pm$ 1.9 (range 2.6–8.3, $n = 27$) in $bcan^{+/+}$ mice and 5.7 $\pm$ 2.7 (range 2.6–15, $n = 28$) in $bcan^{-/-}$ mice. The average SNR of the postAP was 23.6 $\pm$ 16.6 (range 7–80, $n = 27$) in $bcan^{+/+}$ mice and 19.1 $\pm$ 8.2 (range 8.5–40, $n = 28$) in $bcan^{-/-}$ mice. For each single-unit recording, the average complex waveform was computed and the timing of the different subcomponents measured for quantification of the delay between (i) the presynaptic AP and the EPSP (Pre–EPSP delay), (ii) the EPSP and the postsynaptic AP (EPSP–Post delay), and (iii) the presynaptic AP and the postsynaptic AP (Pre–Post delay). The Pre–Post delay was calculated as the time between the positive peak of the presynaptic AP and the positive peak of the postsynaptic AP. Due to the very fast signal transmission at the calyx of Held, the EPSPs and postsynaptic APs were not always identifiable as fully fledged signal components. Then, the time of occurrence of the EPSP was determined by the inflection point of the rising phase of the EPSP–AP complex. We also measured the durations of the pre- and postsynaptic APs by quantifying the time difference between the positive and negative peaks of the respective signals.

The reliability of synaptic transmission was defined as the ratio of transmission failures (i.e. presynaptic potentials that are not followed by a postsynaptic AP) and successful transmission events (i.e. presynaptic potentials

that are followed by a postsynaptic AP). To rule out that potential transmission failures reflect the activity of another neuron and to confirm the single-unit nature of our recordings, we used the independence assessment of potentials (IAP) criterion introduced by Englitz *et al.* (2009). The IAP analysis is based on the assumption that in the case of multiunit recordings individual potentials would violate the refractory period. Recordings that could not be reliably identified as single-unit recordings were excluded from further analysis.

Statistics

Analysis was performed in MATLAB and SigmaPlot (Systat Software, Erkrath, Germany). Data are given as the mean ± SD or ±SEM for normally distributed data. Otherwise medians [1st quartile, 3rd quartile] are reported. For comparison between the two genotypes we used Student's *t* test or the Mann–Whitney rank sum test depending on the distribution of the data. Correlations between two variables were assessed by Spearman's rank correlation.

Results

Complex structure of PNs and expression of the major PN-related proteoglycans remain unchanged in the MNTB in *bcan*$^{-/-}$ mice

First, the structure of PNs in homozygous brevican knockout mice (*bcan*$^{-/-}$) and wild-type littermates (*bcan*$^{+/+}$) was analysed by means of immunohistochemistry. The proteoglycan brevican is prominently

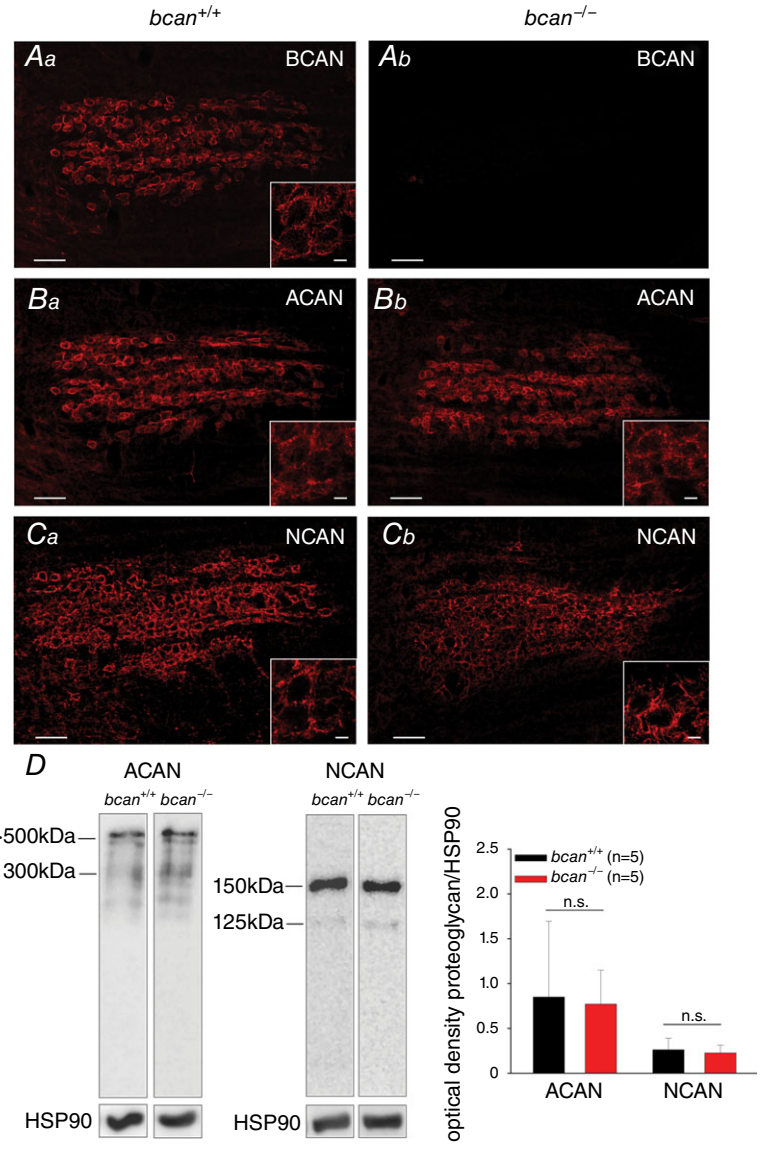

Figure 1. Complex structure of PNs is maintained in the MNTB in *bcan*$^{-/-}$ mice
The structure of PNs in brevican wild-type (*bcan*$^{+/+}$, *Aa*, *Ba*, *Ca*) and knockout mice (*bcan*$^{-/-}$, *Ab*, *Bb*, *Cb*) by means of proteoglycan immunohistochemistry. *A*, in wild-type mice, brevican (BCAN) is prominently expressed and covers nearly every principal neuron (*Aa*), while in *bcan*$^{-/-}$ mice brevican was completely absent (*Ab*). *B* and *C*, no obvious differences in the immunoreactivity of the proteoglycans aggrecan (ACAN) (*B*) and neurocan (NCAN) (*C*) are apparent between both genotypes. Overall, ACAN and NCAN immunohistochemistry shows that the complex structure of the PNs in the MNTB is maintained in *bcan*$^{-/-}$ mice. Scale bar in all MNTB overviews = 100 μm; scale bar in all high magnification insets = 10 μm. *D*, Western blot analysis of major proteoglycans. Protein extracts (35 μg per lane) from homogenized brainstems of 5 *bcan*$^{+/+}$ and 5 *bcan*$^{-/-}$ mice were compared. Samples were subjected to SDS PAGE in a 6% gel. Blots were probed by use of respective antibodies against ACAN and NCAN (left panel). Intensity of chemiluminescence was quantified in relation to the bands of HSP90. Neither aggrecan ($P = 0.7$) nor neurocan ($P = 0.62$) protein levels showed significant differences between *bcan*$^{+/+}$ and *bcan*$^{-/-}$ mice (right panel). Data are given as means ± SD.

expressed in the MNTB of wild-type mice and covers the somata of almost all principal neurons (Fig. 1*Aa*) (Blosa *et al.* 2013), while, as expected, in *bcan*$^{-/-}$ mice brevican was completely absent in the MNTB (Fig. 1*Ab*). Still, the complex structure of the PNs appears to be preserved in brevican-deficient mice as seen from the indistinguishable staining pattern of the other two major components of PNs, aggrecan and neurocan, in both genotypes (Fig. 1*B* and *C*).

In addition to immunohistochemistry, the protein expression levels of aggrecan and neurocan were analysed by means of Western blotting in *bcan*$^{-/-}$ mice and wild-type littermates. The representative blot lanes (Fig. 1*D*, left panel) and the corresponding quantitative density analysis (Fig. 1*D*, right panel) revealed no significant genotype-specific differences in the expression of aggrecan ($P = 0.7$, Mann–Whitney rank sum test) and neurocan ($P = 0.62$, *t* test) in the auditory brainstem.

These data show that perineuronal nets are formed in the MNTB in absence of brevican and that the expression of other major proteoglycans, like aggrecan and neurocan, is virtually unaltered.

Dynamics but not reliability of synaptic transmission are affected in *bcan*$^{-/-}$ mice

Previously, it was shown that in the MNTB brevican is closely associated with the calyx of Held being prominently expressed perisynaptically in close contact with both the pre- and postsynaptic membranes (Blosa *et al.* 2013). The specific localization suggested that brevican might be involved in facilitation of the highly reliable and at the same time extremely fast synaptic transmission at the calyx of Held. Both properties combined are thought to be of high significance for the function of this synapse within the auditory brainstem (Gersdorff & Borst, 2002). To quantify the timing and reliability of excitatory synaptic transmission at this synapse, *in vivo* extracellular single-unit recordings were acquired from MNTB principal cells in brevican-deficient mice and respective wild-type littermates (Fig. 2). The recordings yielded complex voltage signals which were composed of the action potential of the calyx of Held, termed presynaptic AP (preAP) followed by the EPSP and the action potential of the MNTB principal neuron (postAP, Fig. 2*A*). For a detailed analysis of the signals' complex waveform see Sonntag *et al.* (2011).

First, it was tested whether brevican has an influence on the reliability of synaptic transmission at the calyx of Held by quantifying the incidences of transmission failures, i.e. the frequency of occurrence of preAPs not immediately followed by a postAP. The spontaneous discharge activity of 27 MNTB units in control mice (*bcan*$^{+/+}$, Fig. 2*Ba*) and 28 MNTB units in brevican-deficient mice (*bcan*$^{-/-}$, Fig. 2*Bb*) was recorded. The enlargement of two to three

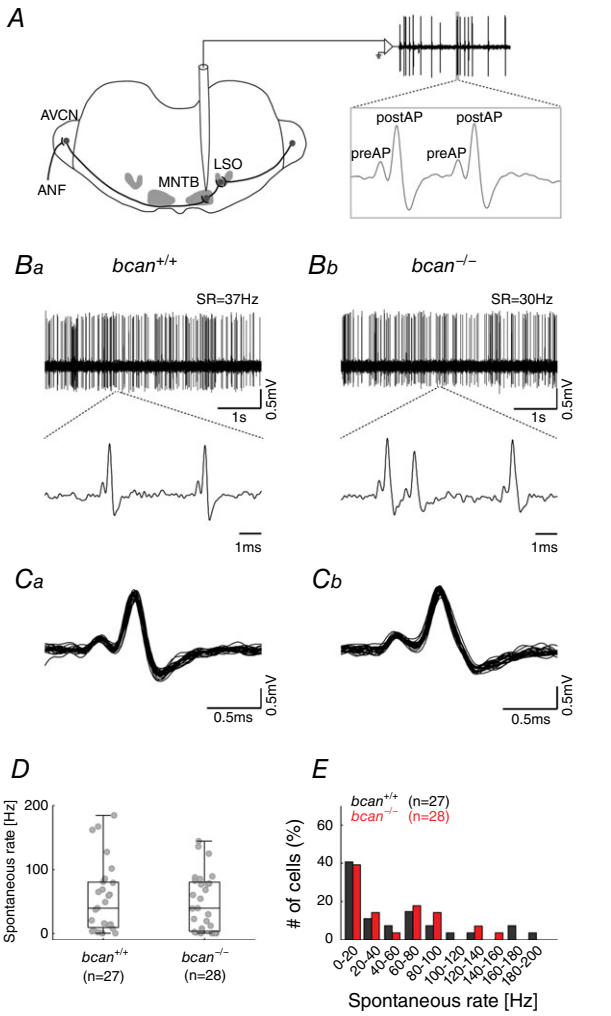

Figure 2. Reliability of synaptic transmission and spontaneous discharge rates are not affected in *bcan*$^{-/-}$ mice
A, extracellular *in vivo* single-unit recordings of MNTB neurons in *bcan*$^{+/+}$ and *bcan*$^{-/-}$ mice. Complex voltage signals were composed of the discharge of the calyx of Held (preAP) and the postsynaptic action potential (postAP, see enlargement of the voltage trace in the inset to the right). Significant numbers of transmission failures, defined as preAPs not followed by postAPs, were detected in neither *bcan*$^{+/+}$ mice nor *bcan*$^{-/-}$ mice. *B*, exemplary voltage traces (5 s, upper panel) of spontaneous activity in a unit of a *bcan*$^{+/+}$ mouse (*Ba*) and a *bcan*$^{-/-}$ mouse (*Bb*). The respective spontaneous discharge rates (SR) were 37 Hz and 30 Hz. Blow-ups of 2–3 individual complex waveforms are shown in the lower panel. *C*, overlay of 25 consecutive signals of a *bcan*$^{+/+}$ unit and a *bcan*$^{-/-}$ unit exemplify the uniformity of the signal waveforms. *D*, spontaneous discharge rates of MNTB principal neurons did not differ between *bcan*$^{+/+}$ and *bcan*$^{-/-}$ mice. *E*, the distribution of spontaneous discharge rates was similar in both genotypes. Forty-one per cent of *bcan*$^{+/+}$ units (black) and 39% of *bcan*$^{-/-}$ units (red) had spontaneous discharge rates <20 Hz. Also, in both genotypes the spontaneous discharge rates were found to cover a broad range (*bcan*$^{+/+}$: 0.2–184 Hz; *bcan*$^{-/-}$: 0.1–144 Hz). Data were obtained from 27 MNTB units in *bcan*$^{+/+}$ mice and 28 MNTB units in *bcan*$^{-/-}$ mice. In *D*, data are presented as median [1st quartile, 3rd quartile]. Abbreviations: ANF, auditory nerve fibre; AVCN, anterior ventral cochlear nucleus; LSO, lateral superior olive; MNTB, medial nucleus of the trapezoid body.

recorded signals (Fig. 2*Ba* and *b*, lower panels) and the overlays of 25 complex waveforms (Fig. 2*Ca* and *b*) did not reveal any transmission failures in MNTB recordings of either genotype. This observation was corroborated by population analysis that failed to show significant transmission failures in 27 and 28 MNTB units of the respective genotypes. A different analysis yielded corresponding results: The postsynaptic spontaneous discharge activity in MNTB recordings did not differ between $bcan^{+/+}$ and $bcan^{-/-}$ mice (median and 1st and 3rd quartiles: 39.7 Hz [9.2, 80.4], $n = 27$ *vs.* 39.3 Hz [3.4, 80.2], $n = 28$, Fig. 2*D*). Also, the distribution of spontaneous discharges was similar in both genotypes (Fig. 2*E*). About half of the units had spontaneous discharge rates <20 Hz ($bcan^{+/+}$: 41%; $bcan^{-/-}$: 39%), which is a characteristic of MNTB principal neurons (Kopp-Scheinpflug *et al.* 2008; Sonntag *et al.* 2009). The spontaneous rates of the units covered a wide range in both genotypes, 0.1–144 Hz in $bcan^{-/-}$ mice and 0.2–184 Hz in $bcan^{+/+}$ mice. Comparable distributions had been reported earlier for CBA/J, C57BL/6 and C3HeB/FeJ mice (Kopp-Scheinpflug *et al.* 2008; Sonntag *et al.* 2009; Sonntag *et al.* 2011) and Mongolian gerbils (Kopp-Scheinpflug *et al.* 2003). Since synaptic transmission was suggested to be less reliable under acoustic stimulation (Kopp-Scheinpflug *et al.* 2003; Lorteije *et al.* 2009), we also compared the reliability of synaptic transmission during sound-evoked activity. The analysis yielded no differences in the transmission reliability between $bcan^{+/+}$ and $bcan^{-/-}$ mice (Fig. 3*A*). However, we observed substantial differences in the shape of excitatory response areas (Fig. 3*B*; $bcan^{+/+}$: top; $bcan^{-/-}$: bottom), which were accompanied by a decrease of the maximum sound-evoked firing rates ($bcan^{+/+}$: 418.1 ± 82.6 Hz, $n = 25$; $bcan^{-/-}$: 249.3 ± 84.1 Hz, $n = 26$; $P < 0.001$, *t* test; Fig. 3*C*) and a prominent reduction of hearing thresholds in $bcan^{-/-}$ mice ($bcan^{+/+}$: 1.2 dB SPL [0, 10.2], $n = 25$; $bcan^{-/-}$: 29.9 dB SPL [10, 51.6], $n = 26$; $P < 0.001$, Mann–Whitney rank sum test; Fig. 3*D*). Since these profound changes in acoustically evoked response properties were not associated with an increase in transmission failures, they are caused by upstream effects rather than by changes at the calyx of Held itself. This issue will be the subject of a separate investigation. With respect to the current study, the present results clearly show that the loss of brevican does not confine the reliability of synaptic transmission at the mature calyx of Held.

Next, $bcan^{+/+}$ and $bcan^{-/-}$ mice were tested for the speed of AP transmission from the calyx of Held synapse to the MNTB principal neuron (Fig. 4). The analysis was based on measurements of the time between the positive peaks of the preAP and the postAP (Pre–Post delay). The overlay of the average of 1137 recorded signals of an exemplary $bcan^{+/+}$ MNTB unit and 917 signals of a $bcan^{-/-}$ unit indicates that the Pre–Post delay is prolonged

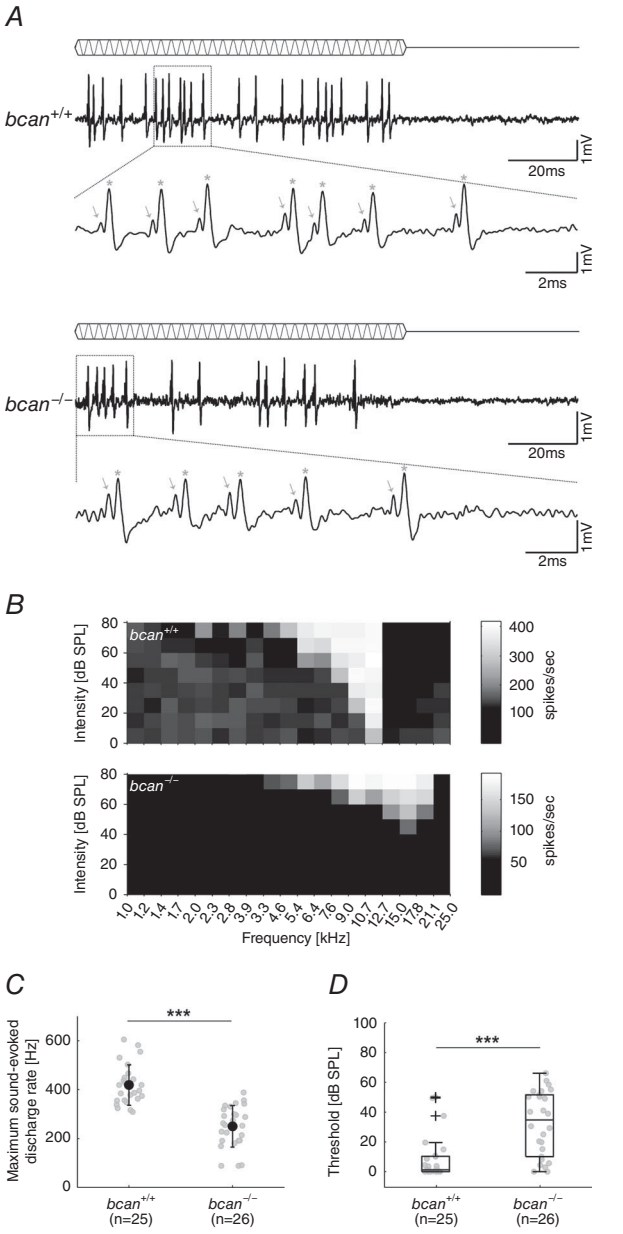

Figure 3. Sound-evoked response properties of MNTB principal cells are altered in $bcan^{-/-}$ mice
A, pure tone stimulation at characteristic frequency and 60 dB SPL in an exemplary MNTB unit of a $bcan^{+/+}$ (top) and a $bcan^{-/-}$ mouse (bottom). The blow-up of individual compound waveforms reveals that in both genotypes all presynaptic potentials (indicated by arrows) are followed by a postsynaptic action potential (indicated by stars), confirming the highly reliable synaptic transmission also under acoustic stimulation. *B*, frequency response areas (20 × 10 frequency–intensity combinations) of two exemplary MNTB principal neurons with similar characteristic frequency; top: $bcan^{+/+}$, bottom: $bcan^{-/-}$. A greyscale was used to encode different discharge rates. *C*, maximum sound-evoked firing rates are significantly reduced in $bcan^{-/-}$ mice compared to respective wild-type animals ($P < 0.001$). *D*, median thresholds at characteristic frequency are significantly elevated in $bcan^{-/-}$ mice ($P < 0.001$). Data were obtained from 25 MNTB units in $bcan^{+/+}$ mice and 26 MNTB units in $bcan^{-/-}$ mice. In *C*, data are presented as means ± SD and in *D*, data are given as median [1st quartile, 3rd quartile]. *P* values: ***$P < 0.001$.

in $bcan^{-/-}$ mice (Fig. 4*A*). The analysis of the entire unit samples revealed a mean Pre–Post delay of 0.46 ± 0.06 ms in $bcan^{-/-}$ mice ($n = 28$), which is significantly longer than the mean Pre–Post delay of 0.40 ± 0.07 ms in $bcan^{+/+}$ mice ($n = 27$, $P < 0.001$, *t* test; Fig. 4*B*). Earlier it was shown that the AP transmission delay at the calyx of Held is highly dependent on the units' discharge rates (Fedchyshyn & Wang 2007; Tolnai *et al.* 2009) with higher firing rates leading to longer transmission delays. Since the spontaneous discharge rates did not differ between control and brevican-deficient mice (Fig. 2*D* and *E*), the slower AP transmission in $bcan^{-/-}$ mice cannot primarily be related to differences in activity levels. A comparative analysis revealed a linear relationship between Pre–Post delay and spontaneous discharge rate for both genotypes ($bcan^{+/+}$: $r = 0.78$, $P < 0.001$; $bcan^{-/-}$: $r = 0.72$, $P < 0.001$; Spearman's rank correlation, Fig. 4*C*) with the Pre–Post delay of $bcan^{-/-}$ units at given spontaneous discharge rates being longer than their $bcan^{+/+}$ counterparts (Fig. 4*C*).

The AP transmission delay is the result of a number of distinct physiological processes, two of which can be quantified in the units' complex waveforms: The first is the time between the preAP and the EPSP (Pre–EPSP delay), which includes the release of the transmitter glutamate from the calyx of Held, the diffusion of the transmitter to the postsynaptic receptors, and the activation of the postsynaptic receptors triggering the EPSP. The second is the time between the EPSP and the postAP (EPSP–Post delay), which reflects the dynamics of postsynaptic AP generation. The respective measurements allowed us to examine whether brevican is involved in any of these two functional complexes. This analysis must consider that in the extracellularly recorded complex waveforms of MNTB units the EPSP is only marginally separated from the postsynaptic AP. The inflection point in the rising phase of the EPSP/AP signal can be used to identify the time of occurrence of the EPSP (Lorteije *et al.* 2009; Kuenzel *et al.* 2011; Sonntag *et al.* 2011). The analysis yielded a significant difference in the Pre–EPSP delay between $bcan^{+/+}$ and $bcan^{-/-}$ animals ($bcan^{+/+}$: 0.31 ± 0.07 ms, $n = 27$; $bcan^{-/-}$: 0.37 ± 0.06 ms, $n = 28$; $P < 0.001$, *t* test, Fig. 4*D*). The quantification of the delay between

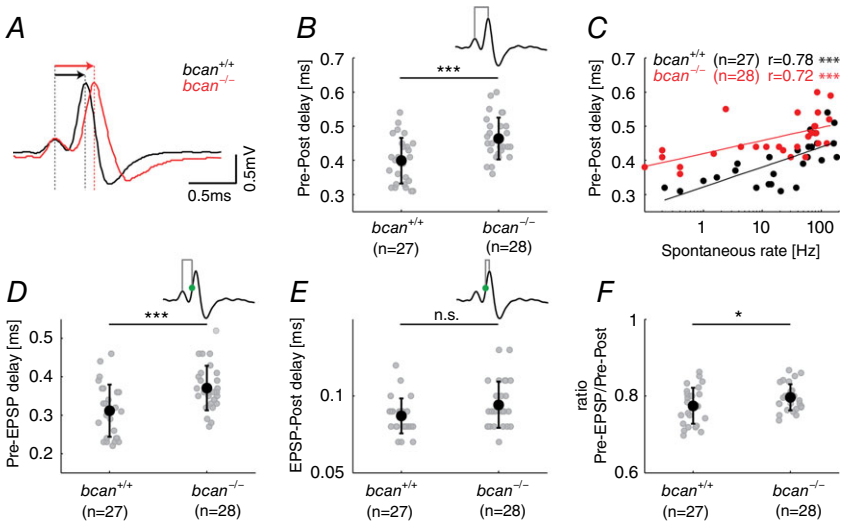

Figure 4. The lack of brevican reduces the speed of AP transmission delay at the calyx of Held
A, average complex waveforms of two exemplary MNTB units ($bcan^{+/+}$: black, $n = 1137$; $bcan^{-/-}$: red, $n = 917$) aligned to the positive peak of the presynaptic AP. The Pre–Post delay, i.e. the time lag between the positive peaks of the preAP and the postAP (red and black arrows above the respective signals), was longer in $bcan^{-/-}$ mice compared to wild-types. *B*, Pre–Post delay of all MNTB units yielded significantly higher values in $bcan^{-/-}$ mice (0.46 ± 0.06 ms) compared to $bcan^{+/+}$ mice (0.4 ± 0.07 ms, $P < 0.001$). *C*, in both genotypes the Pre–Post delay correlates with the spontaneous discharge rates of the units ($bcan^{+/+}$: $r = 0.78$, $P < 0.001$; $bcan^{-/-}$: $r = 0.72$, $P < 0.001$). Still, at given spontaneous rates, units in $bcan^{-/-}$ mice have longer AP transmission delays than in $bcan^{+/+}$ mice. *D* and *E*, AP transmission delay was subdivided into two distinct physiological events: the time between the preAP and the EPSP (Pre–EPSP delay, *D*) and the time from the EPSP to the postAP (EPSP–Post delay, *E*). The time point of the EPSP was defined as the point of inflection on the rising flank of the postsynaptic AP (green dot in the inset). Note that the Pre–EPSP delay was significantly longer in $bcan^{-/-}$ mice (*D*, $bcan^{+/+}$: 0.31 ± 0.07 ms; $bcan^{-/-}$: 0.37 ± 0.06 ms; $P < 0.001$), while the EPSP–Post delay only revealed a tendency for prolongation in knockout mice (*E*, $bcan^{+/+}$: 0.087 ± 0.01 ms; $bcan^{-/-}$: 0.094 ± 0.02 ms; $P = 0.068$). *F*, the ratio of the Pre–EPSP delay and the Pre–Post delay was increased in $bcan^{-/-}$ (0.8 ± 0.01) compared to $bcan^{+/+}$ mice (0.77 ± 0.01, $P < 0.05$), indicating that brevican might have a stronger effect on the speed of Pre–EPSP transmission than on the speed of EPSP–Post transmission. Shown are the values for individual units and the mean ± SD. The analysis was based on the same units shown in Fig. 2. *P* values: ***$P < 0.001$, *$P < 0.05$.

the EPSP and the postAP only showed a tendency for longer transition times in the knockout animals ($bcan^{+/+}$: 0.087 ± 0.01 ms, $n = 27$; $bcan^{-/-}$: 0.094 ± 0.02 ms, $n = 28$; $P = 0.068$, t test, Fig. 4*E*). These data indicate that especially the prolongation of the Pre–EPSP delay accounts for the longer Pre–Post delay. This notion could be further supported by estimating the ratio of the Pre–EPSP delay and the Pre–Post delay. The lack of brevican leads to a significant increase in the fraction of the Pre–EPSP delay relative to the Pre–Post delay ($bcan^{+/+}$: 0.77 ± 0.01, $n = 27$; $bcan^{-/-}$: 0.8 ± 0.01, $n = 28$; $P < 0.05$, t test, Fig. 4*F*).

The clarity of the recorded complex waveform also enabled a quantification of the duration of both the pre-APs and the postAPs and to test for a possible interrelation between the observed prolongation of pre- to postsynaptic transmission delay in $bcan^{-/-}$ units and the characteristics of the respective APs. As a measurement of AP duration, the time from the positive to the negative peak was taken (Fig. 5). Indeed, the increase in transmission delay in knockout mice was associated with a broadening of the preAP as can be seen from the comparison of the mean waveforms of a $bcan^{+/+}$ and a $bcan^{-/-}$ MNTB unit, aligned to the positive peak of the respective preAPs ($bcan^{+/+}$: black, $n = 1137$; $bcan^{-/-}$: red, $n = 917$; Fig. 5*A*). The population analysis corroborated the significantly longer duration of the preAP in $bcan^{-/-}$ units ($bcan^{+/+}$: 0.15 ± 0.03 ms, $n = 27$; $bcan^{-/-}$: 0.18 ± 0.03 ms, $n = 28$; $P < 0.001$, t test, Fig. 5*B*). To rule out that the broadening of the preAP alone accounts for the prolongation of the Pre–EPSP delay, additionally the time between the deflection minimum of the presynaptic potential and the EPSP was quantified. $Bcan^{-/-}$ mice showed significantly longer delays compared to control animals ($bcan^{+/+}$: 0.16 ± 0.05 ms, $n = 27$; $bcan^{-/-}$: 0.19 ± 0.05 ms, $n = 28$; $P < 0.05$, t test). This suggests that both a broader presynaptic AP and a slower depolarization of the postsynaptic membrane account for the longer Pre–EPSP delay in brevican-deficient mice.

An additional analysis yielded that also the postsynaptic APs were broader in $bcan^{-/-}$ mice. This was not so much due to changes in the rising flank of the signals, as to a more shallow decay, as quantified from the interval between the signals' peak values ($bcan^{+/+}$: black, $n = 1137$; $bcan^{-/-}$: red, $n = 917$; Fig. 5*C*). The population data yielded corresponding results affirming significantly broader postAPs in MNTB units of $bcan^{-/-}$ mice (0.37 ± 0.05 ms, $n = 28$) compared to $bcan^{+/+}$ mice (0.31 ± 0.07 ms, $n = 27$, $P < 0.001$, t test, Fig. 5*D*).

Together, these results strongly suggest that the lack of brevican leads to considerable changes in the dynamics of synaptic transmission at the calyx of Held, but also affects both the extracellularly recorded preAPs and postAPs.

Immunoreactivity of receptors and ion channels mediating fast signal transmission is not changed in $bcan^{-/-}$ mice

To achieve the exceptionally fast synaptic transmission, the mature calyces of Held and MNTB principal cells are equipped with specific receptors and ion channels (Gersdorff & Borst, 2002; Schneggenburger & Forsythe, 2006). To test whether the lack of brevican is linked to a disturbance of the respective receptor assembly, we tested a variety of specific antibodies against potassium channel subunits ($K_v1.3$, $K_v3.1\beta$, $K_v2.2$), calcium channel subunits ($Ca_v1.2$, $Ca_v1.3$, $Ca_v2.1$), and glutamate receptor subunits (GluR2/3, GluR4, NMDAR2A). For each channel or receptor subunit, immunostaining was performed in

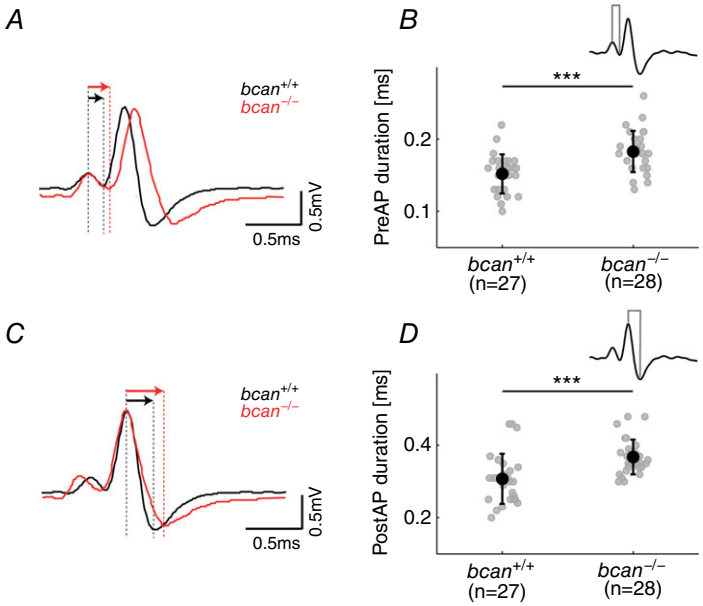

Figure 5. The lack of brevican causes a broadening of pre- and postsynaptic action potentials
A and *C*, average complex waveforms of a $bcan^{+/+}$ MNTB unit (black) and a $bcan^{-/-}$ MNTB unit (red, same units as in Fig. 3) either aligned to the positive peak of the preAP (*A*) or to the positive peak of the postAP (*C*). Differences in signal durations are evidenced from the longer decaying slopes (black *vs.* red; defined as the time difference between positive and negative peaks, indicated by red and black arrows). *B* and *D*, both the presynaptic (*B*) and postsynaptic APs (*D*) were significantly longer in $bcan^{-/-}$ mice ($P < 0.001$). Shown are the values for individual units and means ± SD; same data sample as in Fig. 2. *P* values: ***$P < 0.001$.

three coronal sections from different rostrocaudal nuclear positions, i.e. rostral, central and caudal parts of the MNTB. Figure 6 documents the immunoreactivity against three of the above mentioned antibodies (*A*, $K_v3.1\beta$; *B*, $Ca_v2.1$; *C*, GluR4) in coronal sections at different rostrocaudal nuclear positions; corresponding sections of wild-type and knockout mice are shown to the left and right, respectively. In both genotypes solid immunolabelling was found for $K_v3.1\beta$ (Fig. 6*Aa* and *b*), $Ca_v2.1$ (Fig. 6*Ba* and *b*), and GluR4 (Fig. 6*Ca* and *b*). The same was true for the other tested potassium channel subunits ($K_v1.3$, $K_v2.2$), calcium channel subunits ($Ca_v1.2$, $Ca_v1.3$), and glutamate receptor subunits (GluR2/3, NMDAR2A). The results indicate that brevican deficiency does not have an apparent effect on the composition of receptors and ion channels at the calyx of Held.

The morphology of the calyx of Held is not affected in *bcan*$^{-/-}$ mice

The high speed of synaptic transmission at the calyx of Held is also promoted by the specialized morphology of this synapse. The calyx of Held forms axo-somatic contacts with the principal cell thereby covering ∼50% of the neuron's surface (Kandler & Friauf 1993; Kil *et al.* 1995; Ford *et al.* 2009). During early postnatal development, the calyx of Held morphology changes from an initially cup-like shape to a highly fenestrated appearance. The fenestration of the calyx of Held is believed to be an important structural adaptation for attaining the high speed synaptic transmission (Ford *et al.* 2009). Since brevican was hypothesized to stabilize the interaction between the presynaptic terminal and the postsynaptic neuron (Yamaguchi, 2000), it was obvious to examine whether the lack of brevican results in modifications of the calyx of Held geometry and specifically the state of calyx fenestration. The axosomatic terminals were anterogradely labelled by applying the lipophilic dye NeuroVue Red to the VCN in both *bcan*$^{+/+}$ and *bcan*$^{-/-}$ mice (Fig. 7). Large numbers of marked fibres ascending within the ventral acoustic stria could be followed on their paths to the contralateral MNTB in both wild-type (Fig. 7, left, top) and knockout mice (Fig. 7, left, bottom). The fibres traverse the MNTB horizontally in aggregated bundles of which single fibres bend off either dorsally or ventrally to form at short distances calyx terminals onto MNTB principal neurons. The morphology and state of fenestration of calyx of Held synapses was classified according to the five categories introduced by Ford and coworkers, ranging from 'completely closed structure' (category 1) to 'fully fenestrated appearance' (category 5) (Ford *et al.* 2009; see also Methods). We analysed 30 calyx of Held synapses in two *bcan*$^{+/+}$ mice and 27 calyx of Held synapses in two *bcan*$^{-/-}$ mice from different rostrocaudal and mediolateral positions of the MNTB. The analysis yielded that the majority of calyx terminals were completely fenestrated in both genotypes (category 5, *bcan*$^{+/+}$: 90%; *bcan*$^{-/-}$: 89%). The remaining synapses

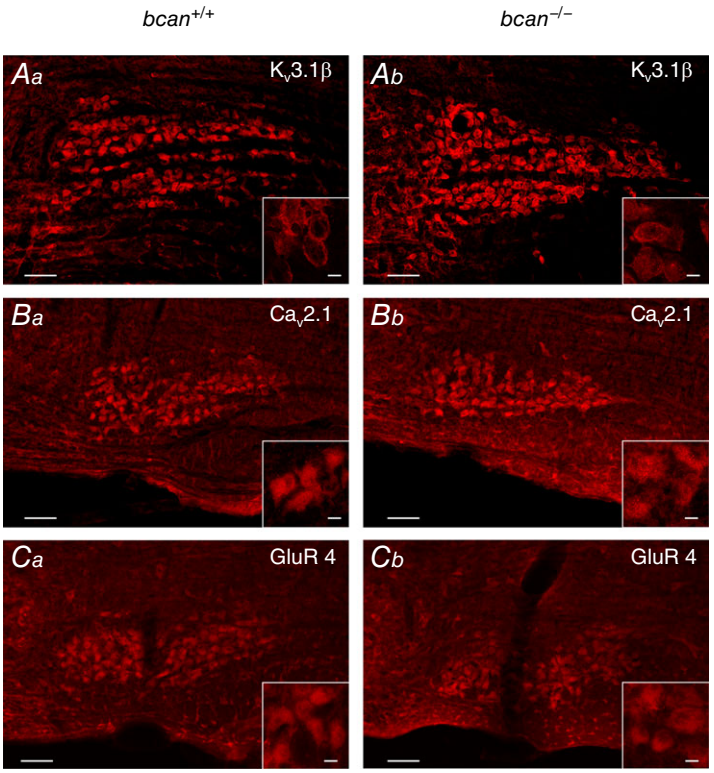

Figure 6. Ion channels and receptors that mediate high-speed transmission are expressed in *bcan*$^{-/-}$ mice
Coronal sections of the ventral lower brainstem dimensioned to include the entire MNTB show the respective immunoreactivity in adult *bcan*$^{+/+}$ (left) and *bcan*$^{-/-}$ mice (right). The rostrocaudal planes of sections in the two genotypes are matched; midline to the left. $K_v3.1\beta$ (*A*), $Ca_v2.1$ (*B*), and GluR4 (*C*); positive immunoreactivity to the antibodies against all three cellular components is seen in the overview staining and in the blow-ups in both genotypes. Scale bar in all MNTB overviews = 100 μm and scale bar in all high magnification inserts = 10 μm.

belong to category 4 ($bcan^{+/+}$: 10%; $bcan^{-/-}$: 11%). These data indicate fully developed calyx of Held morphology in both wild-type and knockout mice (Fig. 7, right panels).

The amount of the glutamate transporter vGlut1 is reduced in $bcan^{-/-}$ mice

The speed of glutamatergic transmission might also be dependent on the fast glutamate recycling mediated by transporters promoting the reuptake of glutamate from the synaptic cleft and the replenishment of synaptic vesicles (Bergles & Edwards, 2008). One of the major vesicular glutamate transporter (vGlut) at the calyx of Held is vGlut1 (Billups, 2005; Blaesse *et al.* 2005; Blosa *et al.* 2013), and it was shown that a reduction of vGlut1 expression correlated with a reduction of the strength of glutamatergic transmission (Wojcik *et al.* 2004; Wilson *et al.* 2005). Given that the reduced speed of synaptic transmission reported here for $bcan^{-/-}$ mice might be linked to deteriorated glutamatergic transmission, the knockout mice were tested for vGlut1 expression using immunohistochemistry. A visual inspection of the slices revealed an even labelling of the calyx terminals throughout the MNTB both in wild-type and knockout mice (Fig. 8*A*, left panels). The vGlut1 labelling also disclosed the same morphological details of the calyx terminals (Fig. 8*A*, right panels) which had been visualized by the anterograde NeuroVue Red labelling shown above. The extensive labelling offered the possibility for a quantitative comparison of vGlut1 expression within the area of the MNTB in wild-type and knockout mice. Coronal sections from three animals of each genotype, including the left and right MNTB and covering the whole of the rostrocaudal and mediolateral nuclear dimension were used for this analysis. Brevican knockout mice showed a significant reduction in the mean vGlut1 labelling ($bcan^{+/+}$: 61 ± 6%, n = 3/6 (mice/MNTB); $bcan^{-/-}$: 40 ± 6%; n = 3/6; $P < 0.001$, t test, Fig. 8*B*). Given these results, it was necessary to exclude that the reduced vGlut1 labelling was due to a general developmental disruption in the $bcan^{-/-}$ mice. To test for this option, we made use of the fact that in rodents PNs are not fully developed before the third-to-fourth postnatal week (Köppe *et al.* 1997; Brückner *et al.* 2000). This enabled an analysis of vGlut1 immunoreactivity in mice of both genotypes at a developmental stage when the adult-like configuration and function of PNs are not yet fully established. The comparison with the data from younger mice then allowed distinction between changes in vGlut1 expression that are mediated by mature PN structures and those which occur before the formation of PNs. The analysis was performed in one $bcan^{-/-}$ and in one $bcan^{+/+}$ mouse at P12. The data revealed no differences between the genotypes (data not shown) providing further evidence that the reduction of vGlut1 in adult mice is indeed related to the lack of brevican.

To exclude that the reduction in vGlut1 is compensated by an upregulation of another vesicular glutamate transporter, we additionally quantified the amount of the vesicular glutamate transporter 2 (vGlut2), which is also found in presynaptic terminals in the MNTB (Billups 2005; Blaesse *et al.* 2005; Blosa *et al.* 2013). No differences in the amount of vGlut2 were found between $bcan^{-/-}$ mice and wild-type animals ($bcan^{+/+}$: 43 ± 7%, n = 3/6 (mice/MNTB); $bcan^{-/-}$: 48 ± 3%; n = 3/6; P = 0.544, t test, Fig. 8*C* and *D*). The same statement also holds for the amount of the glutamate transporter GLT1, which is prominently expressed in glia cells within the MNTB and is thought to also contribute to fast synaptic transmission at the calyx of Held by speeding up the reuptake of glutamate from the synaptic cleft (Ford *et al.* 2009). The amount of GLT1 was not altered in knockout animals ($bcan^{+/+}$: 30 ± 9%, n = 3/6 (mice/MNTB); $bcan^{-/-}$: 29 ± 7%; n = 3/6; P = 0.798, t test).

Thus, it might be concluded that the lack of brevican is specifically linked to a decrease in vGlut1 expression in presynaptic terminals within the MNTB which affects vesicle recycling at the calyx of Held and causes a reduction of the excitatory drive on the MNTB neurons.

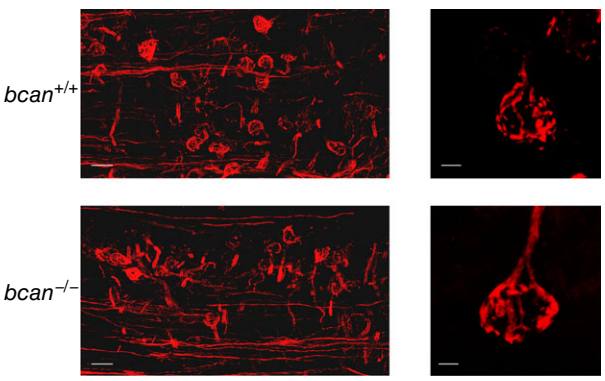

Figure 7. The morphology of the calyx of Held is not affected in $bcan^{-/-}$ mice
Neuronal tracing of the projection from VCN to MNTB and anterograde labelling of the calyx of Held synapses with the lipophilic dye NeuroVue Red. In both $bcan^{+/+}$ (top) and $bcan^{-/-}$ mice (bottom) a large number of traced VCN-derived projections could be targeted (left) showing virtually similar fenestration patterns and morphology of calyces of Held in both genotypes (right). Scale bar in left images = 50 μm, scale bar in right images = 5 μm.

The size of subsynaptic cavities is reduced in $bcan^{-/-}$ mice

Previously brevican immunoreactivity was described to be focally localized close to the somatic surface of principal cells forming ring-like structures around the presynaptic

terminals (Blosa *et al.* 2013). In addition, brevican is also specifically expressed in subsynaptic, extracellular cavities found between the opposing pre- and postsynaptic membranes (Blosa *et al.* 2013). Such subsynaptic cavities were reported to be a typical characteristic of the giant synapses of Held, though different authors use different terminologies: extracellular spaces at calyx of Held and endbulb of Held (Lenn & Reese 1966; Nakajima 1971), extended extracellular spaces at the endbulb of Held (Spirou *et al.* 2005), intermembraneous cisternae at the endbulb of Held (Ryugo *et al.* 2006; Baker *et al.* 2010; Lauer *et al.* 2013), and channel cisterns at the endbulb of Held (Pirone *et al.* 2014). These cavities are frequently found in between two adjacent postsynaptic densities. To date, the function of these cavities is unknown. While Lenn & Reese (1966), who were the first to mention these cavities, considered them to be a fixation artifact, recent reports suggest that they are involved in transmitter recycling (Ryugo *et al.* 2006; Baker *et al.* 2010). To further explore a potential link between brevican expression and the shaping of subsynaptic cavities, transmission electron microscopy was performed at the calyx of Held–MNTB principal junction to analyse the number and size of subsynaptic cavities in mice of both genotypes (Fig. 9*A*). Altogether, 18 ultrathin MNTB sections from different cells of two $bcan^{+/+}$ mice and 28 sections of two $bcan^{-/-}$ mice were used for the analysis. In each section, the number of subsynaptic cavities and their sizes were analysed (see Methods for details). In $bcan^{+/+}$ animals, 0.4 [0.28, 0.54] cavities/μm calyx profile ($n = 18$ calyx profiles) were found with an average size of 0.24 μm^2 [0.14, 0.61] ($n = 88$ cavities). In $bcan^{-/-}$ mice, the extensions of the cavities were significantly reduced (0.09 μm^2 [0.03, 0.16], $n = 152$, $P < 0.001$, Mann–Whitney rank sum test, Fig. 9*B*, right), but their numbers remained unchanged (0.32 [0.17, 0.78] cavities/μm calyx profile, $n = 30$, $P = 0.617$, Mann–Whitney rank sum test, Fig. 9*B*, left). These data suggest that the size of extracellular subsynaptic cavities at the calyx of Held is dependent on the presence of brevican.

Discussion

The calyx of Held is characterized by ultrafast and precisely timed synaptic transmission. The present study provides evidence that the PN component brevican is important for attaining high speed synaptic transmission, but has no effect on the reliability of synaptic transmission. The analysis of complex signal waveforms recorded in the MNTB of $bcan^{-/-}$ mice yielded longer AP transmission delays and broader pre- and postsynaptic APs. The physiological changes in $bcan^{-/-}$ mice were associated with a reduction of vGlut1 expression in the MNTB and with a decrease in the size of extracellular cavities between the pre- and postsynaptic membranes.

In general, the investigation of the physiological function of PNs is challenging, since only specific neurons are surrounded by PNs, and in many brain regions these neurons are intermingled with those that do not express PNs. So, the respective analysis requires the

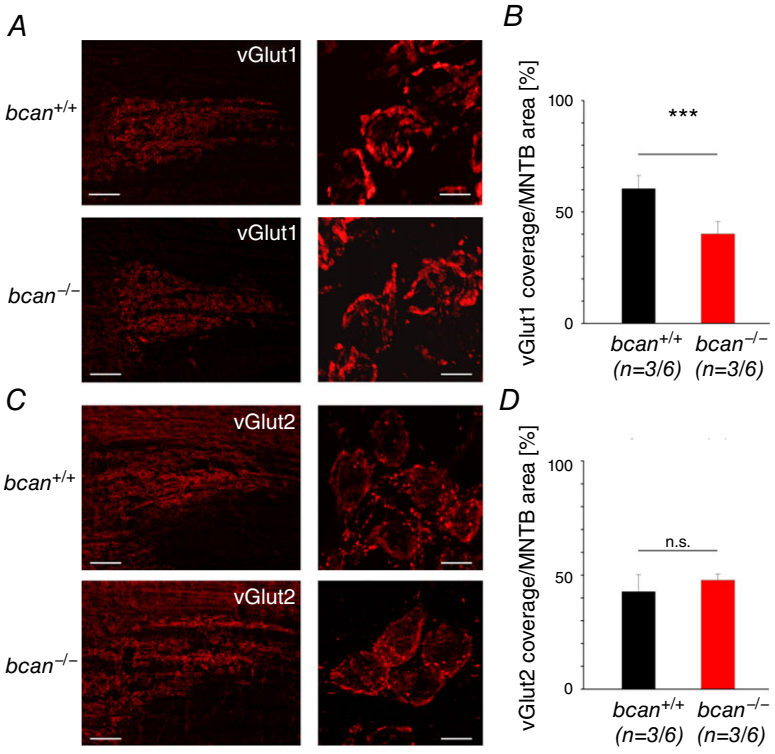

Figure 8. Glutamate transporter vGlut1 is reduced in $bcan^{-/-}$ mice
A, vGlut1 immunohistochemistry in coronal sections of the MNTB (upper panel: $bcan^{+/+}$, lower panel: $bcan^{-/-}$) provides good visualization of the calyces of Held throughout the MNTB (left panels) and also disclosed the typical fenestration patterns in these large axosomatic terminals (right panels, blow-ups). *B*, quantification of the area of the MNTB covered by vGlut1 labelling ($bcan^{+/+}$: black; $bcan^{-/-}$: red; three animals of each genotype, nuclear regions on both sides) yielded a significant reduction in the mean vGlut1 coverage of the MNTB in mutant mice ($P < 0.001$). *C*, respective vGlut2 immunoreactivity in coronal sections of the MNTB; upper panel: $bcan^{+/+}$, lower panel: $bcan^{-/-}$. *D*, quantification of vGlut2 labelling yielded no significant differences between the genotypes in the MNTB ($P = 0.544$). Data are given as means ± SEM. The sample size is given as follows: n = mice/MNTB. *P* values: ***$P < 0.001$. Scale bars in *A* and *C*: left, 100 μm; right, 10 μm.

possibility to clearly distinguish between PN-wearing and PN-negative neurons. In a previous report, the MNTB was introduced as an excellent model system to study the physiological relevance of PNs because of its composition of morphologically and functionally homogeneous neurons virtually all of which are associated with PNs (Blosa *et al.* 2013; Sonntag *et al.* 2015). Also, the MNTB is a well-established model system to investigate the fine-grained mechanisms of synaptic transmission due to the fact that the principal neurons are contacted by the exceptionally large calyx of Held terminals, enabling the simultaneous electrophysiological acquisition of pre- and postsynaptic activities (Gersdorff & Borst 2002; Schneggenburger & Forsythe 2006). Because of these factors, the MNTB offers itself as a unique system to study the role of brevican and potentially of other components of PNs in synaptic transmission.

During development, the calyx of Held and MNTB principal cells undergo structural and functional modifications which as a whole facilitate high-speed synaptic transmission. The mature calyx of Held forms finger-like, axo-somatic contacts with the principal neuron of the MNTB covering ∼50% of the surface of the soma (Morest 1968; Sätzler *et al.* 2002; Hoffpauir *et al.* 2006). This morphological specialization allows for fast and strong depolarization of the postsynaptic membrane, which is a precondition of high-frequency firing and reliable signal transmission (Gersdorff & Borst, 2002; Schneggenburger & Forsythe, 2006). The present immunohistochemical data do not support the notion that disruptions of the calyx of Held morphology in *bcan*$^{-/-}$ mice might be the cause for changes in the dynamics of synaptic transmission. Anterograde labelling of calyx of Held synapses confirmed also for *bcan*$^{-/-}$ mice the formation of the highly fenestrated synaptic morphology, a typical feature of the mature calyx terminal.

Fast and at the same time high-frequency synaptic transmission is further promoted through the incorporation of specific ion channels and receptors in the pre- and postsynaptic membranes, such as the P-type calcium channels

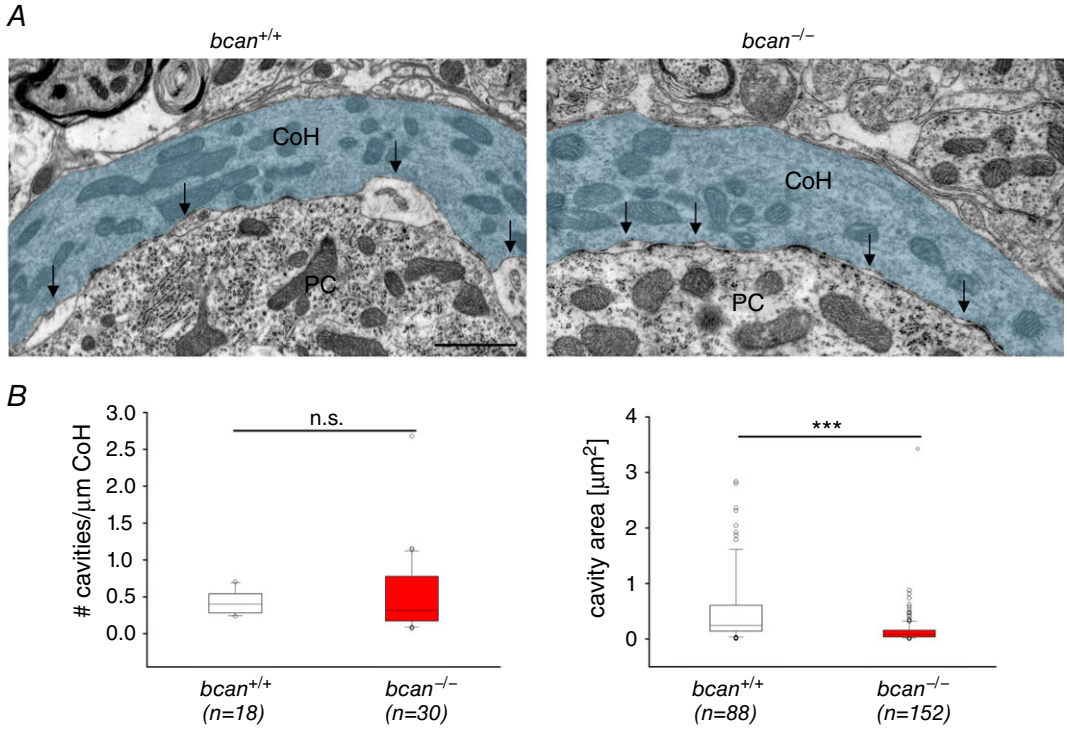

Figure 9. The size of subsynaptic cavities is reduced in *bcan*$^{-/-}$ mice
A, ultrastructural analysis of subsynaptic cavities at the axosomatic calyx of Held in the MNTB of a *bcan*$^{+/+}$ (left) and a *bcan*$^{-/-}$ mouse (right). Subsynaptic, extracellular cavities (arrows) are formed between the opposing membranes of the calyx of Held (CoH, blue) and the principal neuron (PC). These cavities were significantly reduced in size in *bcan*$^{-/-}$ mice compared to *bcan*$^{+/+}$ mice. *B*, quantification of the number (left) and the size (right) of the cavities in both genotypes. The number of cavities which was normalized to the length of the analysed calyx of Held profile was not affected (left, $P = 0.617$), while the size of the subsynaptic cavities was significantly reduced in *bcan*$^{-/-}$ mice ($P < 0.001$). Data were obtained from 18 MNTB sections taken of 2 *bcan*$^{+/+}$ mice and from 28 MNTB sections of 2 *bcan*$^{-/-}$ animals. The analysis yielded 18 calyx of Held profiles with 88 subsynaptic cavities in *bcan*$^{+/+}$ mice and 30 calyx of Held profiles with 152 subsynaptic cavities in *bcan*$^{-/-}$ mice. Data are given as median [1st quartile, 3rd quartile], *P* values: ***$P < 0.001$, scale bar in left image = 1 μm (applies for both images).

formed by the subunit $Ca_v2.1$ (Iwasaki & Takahashi, 1998) and the K_v3 channels which accelerate repolarization and shorten the AP duration (Brew & Forsythe, 1995; Wang *et al.* 1998; Elezgarai *et al.* 2003). The brief presynaptic AP triggers only a short time window for presynaptic calcium influx at the calyx terminal which translates into low release probability of the neurotransmitter glutamate and minor effects of short-term plasticity. Combined, these features guarantee the high reliability of signal transmission at this synapse. To cope with the low release probability and to increase the exocytosis efficiency, the presynaptic calcium channels seem to be tightly coupled with the pool of readily releasable synaptic vesicles (Wang *et al.* 2008; Kochubey *et al.* 2009). Postsynaptically, in the adult system, AMPA receptors mediate fast excitatory postsynaptic potentials through the incorporation of GluR4 subunits (Yang *et al.* 2011), while in the immature system also the slower NMDA receptors contribute to the depolarization (Futai *et al.* 2001; Joshi & Wang, 2002). The presently performed immunohistochemistry did not reveal genotype-specific differences in the expression of the AMPA receptor subunits GluR4 and GluR2/3 as well as in the potassium ($K_v1.3$, $K_v2.2$, $K_v3.1\beta$) and in the calcium channel subunits ($Ca_v1.2$, $Ca_v1.3$, $Ca_v2.1$). Jointly, all these components contribute to the fast synaptic transmission at the calyx of Held (Brew & Forsythe, 1995; Futai *et al.* 2001; Iwasaki & Takahashi, 1998; Johnston *et al.* 2010; Joshi & Wang, 2002; Wang *et al.* 1998; Yang *et al.* 2011; for reviews see: Gersdorff & Borst, 2002; Schneggenburger & Forsythe, 2006). Thus, we conclude that in brevican-deficient mice the basic settings for fast synaptic transmission are not developmentally delayed or altered.

In the MNTB, brevican is primarily expressed in the perisynaptic space and was recently reported to also fill extracellular cavities which are formed in the subsynaptic space between the pre- and postsynaptic membranes (Blosa *et al.* 2013). These cavities are in close proximity to presynaptic release sites and postsynaptic densities and were frequently found between two adjacent postsynaptic densities. The electron microscopic data show that the size of these cavities is reduced in brevican-deficient mice. However, the function of the extracellular cavities and their physiological relevance for high-speed synaptic transmission remains elusive. It was hypothesized that they contribute to transmitter recycling (Ryugo *et al.* 2006; Baker *et al.* 2010) and just this function has also been suggested for the proteoglycan brevican. Specifically, brevican might be involved in the spatial and functional organization of presynaptic release sites (i) by playing a role in controlling the amount of glutamate in the synaptic cleft, (ii) by preventing transmitter spillover, and (iii) through a control of the reuptake of glutamate (Yamada *et al.* 1997; Blosa *et al.* 2013). All these features are crucial for high-frequency synaptic transmission. In brevican knockout mice, the functional consequences of shrinked subsynaptic cavities might be a reduced efficiency of glutamatergic signalling, as evidenced by the prolonged synaptic transmission delay recorded *in vivo*. Mechanistically, this effect could be due to the delayed clearance of glutamate from the synaptic cleft with the residual glutamate rebinding to postsynaptic AMPA receptors, which leads to a desensitization of the receptor (Renden *et al.* 2005; Koike-Tani *et al.* 2008). However, this suggested mechanism and the impact of brevican on glutamate reuptake remain to be experimentally clarified. Glia cells also aid glutamate clearance through respective uptake transporters. However, the quantification of GLT1 fluorescence indicating the abundance of the respective transporter revealed no differences between the genotypes, suggesting that the glial contribution to glutamate clearance may not be affected by the lack of brevican.

Electrophysiological measurements in hippocampal primary neurons of quadruple knockout mice deficient for brevican, neurocan, tenascin-R, and tenascin-C yielded a significantly reduced frequency of miniature EPSCs, which was discussed to reflect modifications in the number of releasable vesicles (Geissler *et al.* 2013). Accordingly, a reduction in the release of glutamate might be a cause for the reduced transmission speed in brevican-deficient mice shown here. In line with this assumption is the reduction in the expression of the vesicular glutamate transporter 1, which, on the one hand, is needed for filling the vesicles with glutamate, and on the other hand, controls the amount of transmitter molecules released from single vesicles (Wojcik *et al.* 2004; Wilson *et al.* 2005). Besides the potential, direct impact on transmitter recycling and vesicular release, brevican might also modulate the activity of individual ion channels and/or receptors in the pre- and postsynaptic membranes (Brakebusch *et al.* 2002) and thereby contribute to the prolongation of synaptic transmission delay. A potential candidate is the potassium channel subunit $K_v3.1$, which was shown to accelerate AP repolarization and promote high-frequency firing. Blocking $K_v3.1$ by TEA leads to broader APs, same as those found in the present study (Brew & Forsythe, 1995; Wang *et al.* 1998; Johnston *et al.* 2010). A functional interplay of brevican and $K_v3.1$ is further supported by the fact that PNs are often found to be associated with $K_v3.1\beta$-positive neurons (Härtig *et al.* 1999). The presently described broadening of the presynaptic AP might largely account for the increase in synaptic transmission delay in $bcan^{-/-}$ mice, since the reduction of the speed of AP repolarization was shown to lead to a delayed and prolonged presynaptic calcium influx which in turn affects the timing of postsynaptic currents (Yang & Wang, 2006). Also the distribution of calcium channels might be influenced by the presence of brevican, i.e. the accumulation of calcium channels close to the active zones which increases synaptic efficacy (Wang *et al.* 2008; Kochubey *et al.* 2009). Taken together, we propose the involvement of brevican in a set

of complex structural and functional interactions affecting the dynamics of synaptic transmission at the calyx of Held. Obviously, brevican has a function in the formation of the fine morphology of calyceal terminals through its expression in subsynaptic cavities. But brevican might also be involved in the control of the expression and/or activity of receptors, ion channels and transporter (e.g. vGlut1). Such divergent functions of brevican were also suggested from changes in the electrophysiological characteristics of CA1 neurons in brevican-deficient mice showing normal initiation of long-term potentiation (LTP) but disturbed LTP maintenance. The respective changes could be mimicked in brainstem slices of wild-type animals treated with anti-brevican antibodies, which points to an active and direct contribution of brevican to signal transmission (Brakebusch *et al.* 2002).

Since the calyx of Held is an important processing station within the auditory pathway, changes in the physiology of this synapse in *bcan*$^{-/-}$ mice raises the question of whether the loss of brevican is associated with hearing deficits. The present single-unit responses of MNTB principals indeed indicate a severe hearing loss in *bcan*$^{-/-}$ mice, reflected by reduction in hearing sensitivity and decrease of maximum sound-evoked discharge rates. However, the MNTB is unlikely to be the source of these deficits, since the reliability of synaptic transmission was not altered, either during spontaneous or during acoustically evoked activity. Since brevican was systemically deleted in the present knockout model, it is likely that the hearing loss originates in lower brainstem processing stations. This seems plausible, since the perineuronal net component brevican is expressed in almost all nuclei of the ascending auditory pathway, and is especially prominent around bushy cells in the cochlear nucleus which provide the input to the MNTB (for review see: Sonntag *et al.* 2015). Given the observed impact of brevican on the synaptic machinery which mediates fast synaptic transmission at the calyx of Held, it seems most likely that the lack of brevican might have similar effects on the synaptic transmission at the endbulbs of Held terminating on globular bushy cells. The respective effects might explain the reduced sound-evoked activity and the deteriorated hearing sensitivity. Thus, the present findings further promote brevican-deficient mice as a promising model system to study the relation between physiological changes in synaptic transmission properties and auditory performance.

In conclusion, our experiments demonstrate the suitability of the MNTB as a powerful experimental *in vivo* model system to study functional aspects of PNs and their constituents in neuronal signalling and synaptic transmission (Blosa *et al.* 2013; Sonntag *et al.* 2015). The present data indicate that brevican specifically helps to attain high-speed synaptic transmission. We conclude that this ECM component modulates glutamatergic synaptic transmission at the calyx of Held, most likely by establishing structurally and functionally separated subsynaptic compartments and by regulating transmitter and vesicle recycling.

References

Baker CA, Montey KL, Pongstaporn T & Ryugo DK (2010). Postnatal development of the endbulb of held in congenitally deaf cats. *Front Neuroanat* **4**, 19.

Bergles DE & Edwards RH (2008). The role of glutamate transporters in synaptic transmission. In *Structural and Functional Organization of the Synapse*, ed. Hell JW, Ehlers & Michael D, pp. 23–61. Springer, New York.

Billups B (2005). Colocalization of vesicular glutamate transporters in the rat superior olivary complex. *Neurosci Lett* **382**, 66–70.

Blaesse P, Ehrhardt S, Friauf E & Nothwang HG (2005). Developmental pattern of three vesicular glutamate transporters in the rat superior olivary complex. *Cell Tissue Res* **320**, 33–50.

Blosa M, Sonntag M, Brückner G, Jäger C, Seeger G, Matthews RT, Rübsamen R, Arendt T & Morawski M (2013). Unique features of extracellular matrix in the mouse medial nucleus of trapezoid body–implications for physiological functions. *Neuroscience* **228**, 215–234.

Borst J & Gerard G (2010). The low synaptic release probability *in vivo*. *Trends Neurosci* **33**, 259–266.

Brakebusch C, Seidenbecher CI, Asztely F, Rauch U, Matthies H, Meyer H, Krug M, Böckers TM, Zhou X, Kreutz MR, Montag D, Gundelfinger ED & Fässler R (2002). Brevican-deficient mice display impaired hippocampal CA1 long-term potentiation but show no obvious deficits in learning and memory. *Mol Cell Biol* **22**, 7417–7427.

Brew HM & Forsythe ID (1995). Two voltage-dependent K^+ conductances with complementary functions in postsynaptic integration at a central auditory synapse. *J Neurosci* **15**, 8011–8022.

Brückner G, Grosche J, Schmidt S, Härtig W, Margolis RU, Delpech B, Seidenbecher CI, Czaniera R & Schachner M (2000). Postnatal development of perineuronal nets in wild-type mice and in a mutant deficient in tenascin-R. *J Comp Neurol* **428**, 616–629.

Brückner G, Szeöke S, Pavlica S, Grosche J & Kacza J (2006). Axon initial segment ensheathed by extracellular matrix in perineuronal nets. *Neuroscience* **138**, 365–375.

Brückner G, Morawski M & Arendt T (2008). Aggrecan-based extracellular matrix is an integral part of the human basal ganglia circuit. *Neuroscience* **151**, 489–504.

Caicedo A & Eybalin M (1999). Glutamate receptor phenotypes in the auditory brainstem and mid-brain of the developing rat. *Eur J Neurosci* **11**, 51–74.

Elezgarai I, Díez J, Puente N, Azkue JJ, Benítez R, Bilbao A, Knöpfel T, Doñate-Oliver F & Grandes P (2003). Subcellular localization of the voltage-dependent potassium channel Kv3.1b in postnatal and adult rat medial nucleus of the trapezoid body. *Neuroscience* **118**, 889–898.

Englitz B, Tolnai S, Typlt M, Jost J & Rübsamen R (2009). Reliability of synaptic transmission at the synapses of Held in vivo under acoustic stimulation. *PLoS ONE* **4**, e7014.

Fedchyshyn MJ & Wang L (2007). Activity-dependent changes in temporal components of neurotransmission at the juvenile mouse calyx of Held synapse. *J Physiol* **581**, 581–602.

Ford MC, Grothe B & Klug A (2009). Fenestration of the calyx of Held occurs sequentially along the tonotopic axis, is influenced by afferent activity, and facilitates glutamate clearance. *J Comp Neurol* **514**, 92–106.

Franklin KBJ & Paxinos G (1997). *The Mouse Brain in Stereotaxic Coordinates.* Academic Press, San Diego.

Frischknecht R & Seidenbecher CI (2012). Brevican: a key proteoglycan in the perisynaptic extracellular matrix of the brain. *Int J Biochem Cell Biol* **44**, 1051–1054.

Futai K, Okada M, Matsuyama K & Takahashi T (2001). High-fidelity transmission acquired via a developmental decrease in NMDA receptor expression at an auditory synapse. *J Neurosci* **21**, 3342–3349.

Gazula V, Strumbos JG, Mei X, Chen H, Rahner C & Kaczmarek LK (2010). Localization of Kv1.3 channels in presynaptic terminals of brainstem auditory neurons. *J Comp Neurol* **518**, 3205–3220.

Geissler M, Gottschling C, Aguado A, Rauch U, Wetzel CH, Hatt H & Faissner A (2013). Primary hippocampal neurons, which lack four crucial extracellular matrix molecules, display abnormalities of synaptic structure and function and severe deficits in perineuronal net formation. *J Neurosci* **33**, 7742–7755.

von Gersdorff H & Borst JGG (2002). Short-term plasticity at the calyx of Held. *Nat Rev Neurosci* **3**, 53–64.

Guinan JJ & Li RY (1990). Signal processing in brainstem auditory neurons which receive giant endings (calyces of Held) in the medial nucleus of the trapezoid body of the cat. *Hear Res* **49**, 321–334.

Härtig W, Derouiche A, Welt K, Brauer K, Grosche J, Mäder M, Reichenbach A & Brückner G (1999). Cortical neurons immunoreactive for the potassium channel Kv3.1b subunit are predominantly surrounded by perineuronal nets presumed as a buffering system for cations. *Brain Res* **842**, 15–29.

Hermann J, Pecka M, von Gersdorff H, Grothe B & Klug A (2007). Synaptic transmission at the calyx of Held under in vivo like activity levels. *J Neurophysiol* **98**, 807–820.

Hoffpauir BK, Grimes JL, Mathers PH & Spirou GA (2006). Synaptogenesis of the calyx of Held: rapid onset of function and one-to-one morphological innervation. *J Neurosci* **26**, 5511–5523.

Hrabetová S, Masri D, Tao L, Xiao F & Nicholson C (2009). Calcium diffusion enhanced after cleavage of negatively charged components of brain extracellular matrix by chondroitinase ABC. *J Physiol* **587**, 4029–4049.

Hsieh CY & Cramer KS (2006). Deafferentation induces novel axonal projections in the auditory brainstem after hearing onset. *J Comp Neurol* **497**, 589–599.

Iwasaki S & Takahashi T (1998). Developmental changes in calcium channel types mediating synaptic transmission in rat auditory brainstem. *J Physiol* **509**, 419–423.

Johnston J, Forsythe ID & Kopp-Scheinpflug C (2010). Going native: voltage-gated potassium channels controlling neuronal excitability. *J Physiol* **588**, 3187–3200.

Joshi I & Wang L (2002). Developmental profiles of glutamate receptors and synaptic transmission at a single synapse in the mouse auditory brainstem. *J Physiol* **540**, 861–873.

Kandler K & Friauf E (1993). Pre- and postnatal development of efferent connections of the cochlear nucleus in the rat. *J Comp Neurol* **328**, 161–184.

Kantor DB, Chivatakarn O, Peer KL, Oster SF, Inatani M, Hansen MJ, Flanagan JG, Yamaguchi Y, Sretavan DW, Giger RJ & Kolodkin AL (2004). Semaphorin 5A is a bifunctional axon guidance cue regulated by heparan and chondroitin sulfate proteoglycans. *Neuron* **44**, 961–975.

Kil J, Kageyama GH, Semple MN & Kitzes LM (1995). Development of ventral cochlear nucleus projections to the superior olivary complex in gerbil. *J Comp Neurol* **353**, 317–340.

Kim M, Chiego DJ & Bradley RM (2008). Ionotropic glutamate receptor expression in preganglionic neurons of the rat inferior salivatory nucleus. *Auton Neurosci* **138**, 83–90.

Klug A (2011). Short-term synaptic plasticity in the auditory brain stem by using in-vivo-like stimulation parameters. *Hear Res* **279**, 51–59.

Kochubey O, Han Y & Schneggenburger R (2009). Developmental regulation of the intracellular Ca^{2+} sensitivity of vesicle fusion and Ca^{2+}-secretion coupling at the rat calyx of Held. *J Physiol* **587**, 3009–3023.

Koike-Tani M, Kanda T, Saitoh N, Yamashita T & Takahashi T (2008). Involvement of AMPA receptor desensitization in short-term synaptic depression at the calyx of Held in developing rats. *J Physiol* **586**, 2263–2275.

Köppe G, Brückner G, Brauer K, Härtig W & Bigl V (1997). Developmental patterns of proteoglycan-containing extracellular matrix in perineuronal nets and neuropil of the postnatal rat brain. *Cell Tissue Res* **288**, 33–41.

Kopp-Scheinpflug C, Lippe WR, Dörrscheidt GJ & Rübsamen R (2003). The medial nucleus of the trapezoid body in the gerbil is more than a relay: comparison of pre- and postsynaptic activity. *J Assoc Res Otolaryngol* **4**, 1–23.

Kopp-Scheinpflug C, Tolnai S, Malmierca MS & Rübsamen R (2008). The medial nucleus of the trapezoid body: comparative physiology. *Neuroscience* **154**, 160–170.

Kuenzel T, Borst J, Gerard G & vander Heijden M (2011). Factors controlling the input-output relationship of spherical bushy cells in the gerbil cochlear nucleus. *J Neurosci* **31**, 4260–4273.

Lauer AM, Connelly CJ, Graham H & Ryugo DK (2013). Morphological characterization of bushy cells and their inputs in the laboratory mouse (*Mus musculus*) anteroventral cochlear nucleus. *PloS ONE* **8**, e73308.

Lenn NJ & Reese TS (1966). The fine structure of nerve endings in the nucleus of the trapezoid body and the ventral cochlear nucleus. *Am J Anat* **118**, 375–389.

Lorteije JAM, Rusu SI, Kushmerick C & Borst JGG (2009). Reliability and precision of the mouse calyx of Held synapse. *J Neurosci* **29**, 13770–13784.

Lv P, Kim HJ, Lee J, Sihn C, Fathabad Gharaie S, Mousavi-Nik A, Wang W, Wang H, Gratton MA, Doyle KJ, Zhang X, Chiamvimonvat N & Yamoah EN (2014). Genetic, cellular, and functional evidence for Ca^{2+} inflow through $Ca_v1.2$ and $Ca_v1.3$ channels in murine spiral ganglion neurons. *J Neurosci* **34**, 7383–7393.

Mallmann RT, Elgueta C, Sleman F, Castonguay J, Wilmes T, van den Maagdenberg, Arn & Klugbauer N (2013). Ablation of Ca(V)2.1 voltage-gated Ca^{2+} channels in mouse forebrain generates multiple cognitive impairments, *PLoS ONE* **8**, e78598; DOI: 10.1371/journal.pone.0078598.

Matthews RT, Gary SC, Zerillo C, Pratta M, Solomon K, Arner EC & Hockfield S (2000). Brain-enriched hyaluronan binding (BEHAB)/brevican cleavage in a glioma cell line is mediated by a disintegrin and metalloproteinase with thrombospondin motifs (ADAMTS) family member. *J Biol Chem* **275**, 22695–22703.

Matthews RT, Kelly GM, Zerillo CA, Gray G, Tiemeyer M & Hockfield S (2002). Aggrecan glycoforms contribute to the molecular heterogeneity of perineuronal nets. *J Neurosci* **22**, 7536–7547.

McRae PA, Rocco MM, Kelly G, Brumberg JC & Matthews RT (2007). Sensory deprivation alters aggrecan and perineuronal net expression in the mouse barrel cortex. *J Neurosci* **27**, 5405–5413.

Milev P, Maurel P, Chiba A, Mevissen M, Popp S, Yamaguchi Y, Margolis RK & Margolis RU (1998). Differential regulation of expression of hyaluronan-binding proteoglycans in developing brain: aggrecan, versican, neurocan, and brevican. *Biochem Biophys Res Commun* **247**, 207–212.

Morales E, Fernandez FR, Sinclair S, Molineux ML, Mehaffey WH & Turner RW (2004). Releasing the peri-neuronal net to patch-clamp neurons in adult CNS. *Pflugers Arch* **448**, 248–258.

Morawski M, Dityatev A, Hartlage-Rübsamen M, Blosa M, Holzer M, Flach K, Pavlica S, Dityateva G, Grosche J, Brückner G & Schachner M (2014). Tenascin-R promotes assembly of the extracellular matrix of perineuronal nets via clustering of aggrecan: insights from tenascin-R deficient neural cultures. *Philos Trans R Soc Lond B Biol Sci* **369**, 20140046.

Morest DK (1968). The growth of synaptic endings in the mammalian brain: a study of the calyces of the trapezoid body. *Z Anat Entwicklungsgesch* **127**, 201–220.

Nakajima Y (1971). Fine structure of the medial nucleus of the trapezoid body of the bat with special reference to two types of synaptic endings. *J Cell Biol* **50**, 121–134.

Nakamura PA & Cramer KS (2013). EphB2 signaling regulates lesion-induced axon sprouting but not critical period length in the postnatal auditory brainstem. *Neural Dev* **8**, 2.

Pines G, Danbolt NC, Bjørås M, Zhang Y, Bendahan A, Eide L, Koepsell H, Storm-Mathisen J, Seeberg E & Kanner BI (1992). Cloning and expression of a rat brain L-glutamate transporter. *Nature* **360**, 464–467.

Pirone A, Kurt S, Zuccotti A, Rüttiger L, Pilz P, Brown DH, Franz C, Schweizer M, Rust MB, Rübsamen R, Friauf E, Knipper M & Engel J (2014). $\alpha 2\delta 3$ is essential for normal structure and function of auditory nerve synapses and is a novel candidate for auditory processing disorders. *J Neurosci* **34**, 434–445.

Rauch U, Clement A, Retzler C, Fröhlich L, Fässler R, Göhring W & Faissner A (1997). Mapping of a defined neurocan binding site to distinct domains of tenascin-C. *J Biol Chem* **272**, 26905–26912.

Renden R, Taschenberger H, Puente N, Rusakov DA, Duvoisin R, Wang L, Lehre KP & von Gersdorff H (2005). Glutamate transporter studies reveal the pruning of metabotropic glutamate receptors and absence of AMPA receptor desensitization at mature calyx of held synapses. *J Neurosci* **25**, 8482–8497.

Ryugo DK, Montey KL, Wright AL, Bennett ML & Pongstaporn T (2006). Postnatal development of a large auditory nerve terminal: the endbulb of Held in cats. *Hear Res* **216–217**, 100–115.

Suttkus A, Rohn S, Weigel S, Glöckner P, Arendt T & Morawski M (2014). Aggrecan, link protein and tenascin-R are essential components of the perineuronal net to protect neurons against iron-induced oxidative stress. *Cell Death Dis* **5**, e1119; DOI: 10.1038/cddis.2014.25.

Sätzler K, Söhl LF, Bollmann JH, Borst JGG, Frotscher M, Sakmann B & Lübke JHR (2002). Three-dimensional reconstruction of a calyx of Held and its postsynaptic principal neuron in the medial nucleus of the trapezoid body. *J Neurosci* **22**, 10567–10579.

Schneggenburger R & Forsythe ID (2006). The calyx of Held. *Cell Tissue Res* **326**, 311–337.

Sonntag M, Englitz B, Kopp-Scheinpflug C & Rübsamen R (2009). Early postnatal development of spontaneous and acoustically evoked discharge activity of principal cells of the medial nucleus of the trapezoid body: an *in vivo* study in mice. *J Neurosci* **29**, 9510–9520.

Sonntag M, Englitz B, Typlt M & Rübsamen R (2011). The calyx of held develops adult-like dynamics and reliability by hearing onset in the mouse *in vivo*. *J Neurosci* **31**, 6699–6709.

Sonntag M, Blosa M, Schmidt S, Rübsamen R & Morawski M (2015). Perineuronal nets in the auditory system. *Hear Res* doi: 10.1016/j.heares.2014.12.012.

Spirou GA, Rager J & Manis PB (2005). Convergence of auditory-nerve fiber projections onto globular bushy cells. *Neuroscience* **136**, 843–863.

Takamori S, Rhee JS, Rosenmund C & Jahn R (2000). Identification of a vesicular glutamate transporter that defines a glutamatergic phenotype in neurons. *Nature* **407**, 189–194.

Thiers FA, Nadol JB & Liberman MC (2008). Reciprocal synapses between outer hair cells and their afferent terminals: evidence for a local neural network in the mammalian cochlea. *J Assoc Res Otolaryngol* **9**, 477–489.

Tolnai S, Englitz B, Scholbach J, Jost J & Rübsamen R (2009). Spike transmission delay at the calyx of Held in vivo: rate dependence, phenomenological modeling, and relevance for sound localization. *J Neurophysiol* **102**, 1206–1217.

Tong H, Kopp-Scheinpflug C, Pilati N, Robinson SW, Sinclair JL, Steinert JR, Barnes-Davies M, Allfree R, Grubb BD, Young SM & Forsythe ID (2013). Protection from noise-induced hearing loss by Kv2.2 potassium currents in the central medial olivocochlear system. *J Neurosci* **33**, 9113–9121.

Typlt M, Haustein MD, Dietz B, Steinert JR, Witte M, Englitz B, Milenkovic I, Kopp-Scheinpflug C, Forsythe ID & Rübsamen R (2010). Presynaptic and postsynaptic origin of multicomponent extracellular waveforms at the endbulb of Held-spherical bushy cell synapse. *Eur J Neurosci* **31**, 1574–1581.

Vigetti D, Andrini O, Clerici M, Negrini D, Passi A & Moriondo A (2008). Chondroitin sulfates act as extracellular gating modifiers on voltage-dependent ion channels. *Cell Physiol Biochem* **22**, 137–146.

Vitellaro-Zuccarello L, Bosisio P, Mazzetti S, Monti C & Biasi S de (2007). Differential expression of several molecules of the extracellular matrix in functionally and developmentally distinct regions of rat spinal cord. *Cell Tissue Res* **327**, 433–447.

Wang LY, Gan L, Forsythe ID & Kaczmarek LK (1998). Contribution of the Kv3.1 potassium channel to high-frequency firing in mouse auditory neurons. *J Physiol* **509**, 183–194.

Wang LY, Neher E & Taschenberger H (2008). Synaptic vesicles in mature calyx of Held synapses sense higher nanodomain calcium concentrations during action potential-evoked glutamate release. *J Neurosci* **28**, 14450–14458.

Wilson NR, Kang J, Hueske EV, Leung T, Varoqui H, Murnick JG, Erickson JD & Liu G (2005). Presynaptic regulation of quantal size by the vesicular glutamate transporter VGLUT1. *J Neurosci* **25**, 6221–6234.

Wojcik SM, Rhee JS, Herzog E, Sigler A, Jahn R, Takamori S, Brose N & Rosenmund C (2004). An essential role for vesicular glutamate transporter 1 (VGLUT1) in postnatal development and control of quantal size. *Proc Natl Acad Sci USA* **101**, 7158–7163.

Yamada H, Fredette B, Shitara K, Hagihara K, Miura R, Ranscht B, Stallcup WB & Yamaguchi Y (1997). The brain chondroitin sulfate proteoglycan brevican associates with astrocytes ensheathing cerebellar glomeruli and inhibits neurite outgrowth from granule neurons. *J Neurosci* **17**, 7784–7795.

Yamaguchi Y (2000). Lecticans: organizers of the brain extracellular matrix. *Cell Mol Life Sci* **57**, 276–289.

Yang YM & Wang LY (2006). Amplitude and kinetics of action potential-evoked Ca^{2+} current and its efficacy in triggering transmitter release at the developing calyx of Held synapse. *J Neurosci* **26**, 5698–5708.

Yang YM, Aitoubah J, Lauer AM, Nuriya M, Takamiya K, Jia Z, May BJ, Huganir RL & Wang LY (2011). GluA4 is indispensable for driving fast neurotransmission across a high-fidelity central synapse. *J Physiol* **589**, 4209–4227.

Additional information

Competing interests

The authors declare that they have no competing interest.

Author contributions

M.B., M.S., R.R. and M.M designed the research; M.B. and M.S. performed the electrophysiological experiments and analysed the data; M.B., M.S., C.J. and S.W. performed the immunohistochemical and Western blot experiments and analysed the data; M.B., J.S. and M.M. carried out the electron microscopy and analysed the data; R.F., C.S., R.T.M and T.A. participated in the interpretation of the data and revised the manuscript; the paper was written by M.B., M.S., R.R. and M.M. and the research was conducted at the University of Leipzig. All authors approved the final version of the manuscript for publication.

Funding

The project was supported by the Priority Program 1608 "Ultrafast and temporally precise information processing: normal and dysfunctional hearing" of the Deutsche Forschungsgemeinschaft (grant Mo2249/2-1 and Ru390/20-1), by the EU-COST Action BM1001 'Brain Extracellular Matrix in Health and Disease', the Alzheimer Forschungsinitiative e.V. (AFI no. 11861) and by the European Union and the Federal State of Saxony to M.M., by the Schram foundation (T287/21796/2011 to R.F.) and the German Research Foundation (GRK1167 to C.I.S.).

Acknowledgements

We are very grateful to Bernhard Englitz for invaluable discussions of the present data.